Cancer Letters 630 (2025) 217907

Contents lists available at ScienceDirect

Cancer Letters

journal homepage: www.elsevier.com/locate/canlet

Original Articles

NF-κB-mediated cytokine secretion and glutamate metabolic reprogramming converge in breast cancer brain tropism

Sara Di Russo [a], Giulia Elizabeth Borsatti [a], Amani Bouzidi [a,b], Francesca Romana Liberati [a,c], Agnese Riva [a], Farida Tripodi [d], Lucrezia Romana Rolfi [a], Sharon Spizzichino [a], Antonella Tramutola [a], Marzia Perluigi [a], Daniela Trisciuoglio [e], Giorgio Giardina [a], Alessandro Paiardini [a], Paola Coccetti [d], Serena Rinaldo [a], Francesca Cutruzzolà [a,f,1], Alessio Paone [f,*,1]

[a] Department of Biochemical Sciences A. Rossi Fanelli, Sapienza University of Rome, P.le A. Moro 5, 00185, Rome, Italy
[b] Regina Elena Institute - Istituti Fisioterapici Ospitalieri (IRE), Department of Experimental Oncology, Via Chianesi 53, 00144, Rome, Italy
[c] IRCCS Humanitas Research Hospital, Via Manzoni 56, 20089, Milan, Italy
[d] Department of Biotechnology and Biosciences, University of Milano-Bicocca, Milano, Italy. Piazza della Scienza 2, 20126, Milan, Italy
[e] IBPM Institute of Molecular Biology and Pathology, CNR National Research Council of Italy, Via degli Apuli 4, 00185, Rome, Italy
[f] Department of Biochemical Sciences A. Rossi Fanelli, Sapienza University of Rome, Laboratory Affiliated to Istituto Pasteur Italia-Fondazione Cenci Bolognetti, P.le A. Moro 5, 00185, Rome, Italy

ARTICLE INFO

Keywords:
Breast cancer
Brain metastasis
NF-κB signaling
Blood-brain barrier
Glutamate
Inflammation

ABSTRACT

Brain metastases are an increasingly common and life-threatening complication of breast cancer. Here, we report that breast cancer cells with a propensity for cerebral colonization (BrM cells) display a distinct imbalance in the NF-κB pathway characterized by elevated IKKβ and reduced IKKα levels. This imbalance reduces the levels of the downstream NF-κB modulators IκBα and TAX1BP1, fostering a chronically active pro-inflammatory program. Such BrM cells secrete high concentrations of IL-8 and GRO chemokines, enhancing blood–brain barrier permeability *in vitro* and triggering astrocyte activation *in vivo*. In parallel, we observed that the altered NF-κB signaling increases the expression of glutamate transporters EAAT1 and EAAT2, which allows BrM cells to uptake and utilize glutamate, a neurotransmitter readily available in the brain, as a key energy source. Analysis of energy metabolism confirms a pronounced reliance on glutamate for both oxidative phosphorylation and glycolysis, which correlates with an increased migratory and invasive capacity. Importantly, pharmacological inhibition of glutamate import curtails *in vitro* migratory ability and reduces the formation of brain lesions in a murine model.

Our study thus highlights a dual strategy employed by BrM cells, whereby they orchestrate a pro-inflammatory milieu to breach the BBB and simultaneously exploit glutamate metabolism to sustain invasiveness. These findings highlight the inflammatory–metabolic axis as a promising target for therapeutic or preventive strategies against breast cancer progression to the brain.

1. Introduction

Breast cancer continues to be the most prevalent type of cancer among women predicted for 2024 and the second leading cause of cancer-related deaths in these patients [1]. The most severe manifestation of this pathology is brain metastases, which are increasing due mainly to longer survival rates in women with metastatic breast cancer (MBC). Women with HER2^{+} or triple-negative MBC, which make up 30–40 % of cases, face a particularly high risk of developing brain metastases. Studies indicate that 30–50 % of women with these high-risk subtypes will develop and die from CNS complications [2]. The prognosis for these patients is poor, also because the blood-brain barrier (BBB), which normally limits the entry of molecules and cells into the brain, also restricts access to therapeutic agents and reduces the

* Corresponding author.
E-mail address: alessio.paone@uniroma1.it (A. Paone).
[1] These authors contributed equally.

https://doi.org/10.1016/j.canlet.2025.217907
Received 10 April 2025; Received in revised form 20 June 2025; Accepted 7 July 2025
Available online 8 July 2025

effectiveness of standard therapies [3]. Notably, despite the effectiveness of the BBB, certain tumors preferentially metastasize to the brain rather than to other organs with more permissive endothelial barriers [4]. The journey of circulating tumor cells (CTCs) to the brain is constrained by a peculiar microenvironment represented by small-caliber capillaries with distinctive structural and functional characteristics, whose interactions with tumor cells, described in detail below, play a key role in facilitating or hindering their passage. CTCs, which often have diameters exceeding that of cerebral microcapillaries, can become lodged in these vessels, aided by adhesion molecules expressed by both the tumor cells and the brain endothelium. This creates a distinct "local microenvironment" where tumor cells and endothelial cells remain in tight contact, accumulating secreted factors from both sides that can promote metastatic progression. Moreover, CTCs may travel in clusters rather than as single cells, further slowing or obstructing capillary transit and intensifying cell–cell interactions within the cerebral vasculature. It has been hypothesized that only a relatively small subset of CTCs with specific characteristics can successfully infiltrate the brain and give rise to secondary tumors. Consequently, the cells truly responsible for metastasis formation undergo a selection process. Nevertheless, the precise nature of the traits under selection that determine effective metastatic potential remains elusive [5]. Inflammatory cytokines such as TNF and IL6 are frequently produced directly by cancer cells and are implicated in promoting cell survival and proliferation pathways [4]. These molecules could also be involved in processes that mimic the mechanisms utilized by the immune system to penetrate the brain and combat infections [6]. This suggests that specific cytokine-mediated events that trigger immune cells to breach the BBB may similarly enable cancer cells to invade and colonize the parenchyma of brain [6]. The brain's metabolic profile, rich in neurotransmitters like glutamate and branched-chain amino acids (BCAAs), and characterized by an active uptake of glucose by neural cells, leaving limited availability for other cell types, plays a critical role in the adaptation and survival of metastatic cancer cells [7]. Glutamate, abundant in the brain, can be metabolized into α-ketoglutarate, an essential intermediate in the tricarboxylic acid (TCA) cycle crucial for ATP generation [8]. Recent studies have also highlighted the role of amino acids such as serine and glycine in increasing the chemokinetic ability of lung cancer cells, most likely by enhancing ATP production and reducing reactive oxygen species (ROS), thus probably facilitating tissue invasion and adaptation to the brain's metabolic environment [9]. Here, we demonstrate that breast cancer cell lines with a propensity for brain metastasis, namely the human MDA-MB-231 BrM (231BrM) line and the murine 4TI BrM and E0771 BrM lines (collectively referred to as BrM cells or 'brain-seeking cells'), exhibit a specific alteration in the NF-κB pathway when compared to the parental lines from which they were derived (respectively MDA-MB-231 (231), 4T1 and E0771). These BrM derivatives were specifically selected for their well-documented ability to spontaneously form brain metastases when injected into mice, a feature that reflects the key biological process we aimed to investigate. This alteration in the NF-κB pathway leads to a specific inflammatory profile that not only efficiently breaches an *in vitro* model of brain microvascular endothelial cells, mimicking the blood-brain barrier, but also supports a mechanism that increases glutamate uptake and utilization. Ultimately, the increased glutamate utilization is crucial for the invasion of these cells into the brain tissue *in vivo*.

2. Materials and methods

2.1. Cell lines

The original parental cells are MDA-MB-231 (231) (developed into brain metastatic 231BrM [10]) were both provided by Dr. J. Massaguè from Memorial Sloan Kettering Institute, New York; USA, 4T1 (developed into brain metastatic 4T1BrM [11]) were both provided by Dr. M. Lorger from University of Leeds, Leeds; UK and E0771 (developed into brain metastatic E0771BrM [12]) were both provided by Dr. M. Valiente from Centro Nacional de Investigaciones Oncológicas, Madrid; Spain. 231, 231BrM, 4T1, 4T1BrM cells were grown in RPMI medium (SIAL-RPMI-A), supplemented with 100 IU/ml penicillin-streptomycin (P4458-100; Sigma-Aldrich) and 10 % fetal bovine serum (FBS-12A; Capricorn). E0771 were grown in RPMI medium (SIAL-RPMI-A), supplemented with 100 IU/ml penicillin-streptomycin (P4458-100; Sigma-Aldrich), 10 % fetal bovine serum (FBS-12A; Capricorn), and 1 % HEPES (H0887-100 ml Sigma-Aldrich). HCMEC/D3 were purchased from Merck KGaA (Darmstadt, Germany) and seeded on plastic cell culture plates coated with collagen (C-3867-1vl; Sigma-Aldrich) and grown in Endothelial Cell Base Medium, (PC-22210; Promo Cell), supplemented with 100 IU/ml penicillin-streptomycin (P4458-100; Sigma-Aldrich/Merck) and SupplementPack Endothelial Cell Growth Medium (C-39210; Promo Cell, Heidelberg, Germany). All cells were maintained under standard incubation conditions at 37 °C with 5 % carbon dioxide.

2.2. RNA extraction, reverse transcription, and quantitative real-time PCR analysis

Total RNA was extracted from cells using TRIzol reagent (QG79306, Qiagen) following the manufacturer's instructions. Reverse transcription reactions were performed on 1 μg of total RNA with High-Capacity cDNA Reverse Transcription Kit (4368814, Thermo Fisher Scientific). Each qPCR tube contained 5 μl Sybr SensiFAST Lo-ROX KIT (BIO-94005, Meridian Bioscience, Villa Cortese, Italy), 0.4 μl primer forward 10 μM, 0.4 μl primer reverse 10 μM, 1 μl complementary DNA (1:10 diluted) and 3.2 μl nuclease-free water (129,115, Qiagen), to achieve the final volume 10 μl. Reactions were performed using QuantStudio 3 by Applied Biosystems (Thermo Fisher Scientific). The cycling protocol was 50 °C for 2 min 95 °C for 2 min, 40 cycles of 95 °C for 5 s, 60 °C for 30 s, before fluorescence detection. A melting curve was determined using the standard instrument protocol. Amplification specificity was assessed by analysis of melting curves. Relative fold change of the expression of individual genes was calculated using the $2^{-\Delta\Delta Ct}$. ΔCt is calculated as difference between Ct of each gene and Ct of β-actin gene, used as normalizer. Each sample was analyzed in triplicate. Primer sequences are shown in Table 1.

2.3. Human astrocytes generation

Neural stem cells (NSCs) were differentiated into astrocytes as previously described [13]. NSCs were seeded at 25,000 cells/cm^2 density on Geltrex (Thermo Fisher Scientific Inc., MA, United States 12,760)-coated plates in astrocytes medium, composed of DMEM 1X (Thermo Fisher 11, 995), 1 % fetal bovine serum ES qualified (Thermo Fisher 16,141), 2 mM Glutamax (Thermo Fisher 35,050), 1 % N2 supplement (Thermo Fisher 17,502) and 1X antibiotic antimycotic solution (Thermo Fisher 15,240). When the cells reached 90–95 % confluency, they were split to the initial

Table 1
Primer sequences used for qPCR amplification.

Gene	Species	Primer Direction	Sequence
CXCR1	**Human**	**Forward (FW)**	**AGGTTGTGTGTGGAAGGTGA**
CXCR1	**Human**	**Reverse (RW)**	**CCCTGAAGACACCAGTTCCT**
CXCR2	**Human**	**Forward (FW)**	**CCCCTCATCTACGCCTTCAT**
CXCR2	**Human**	**Reverse (RW)**	**GAGTAGTGGAAGTGTGCCCT**
CXCR1	**Mouse**	**Forward (FW)**	**ACACCTGTAGCCTAACCCAC**
CXCR1	**Mouse**	**Reverse (RW)**	**AGGACAGAAAGCTCCCAGAC**
CXCR2	**Mouse**	**Forward (FW)**	**CTCGGGGTTCCTTCTTGTCT**
CXCR2	**Mouse**	**Reverse (RW)**	**CGTGACCTCTTTCTCCCTGT**
β-ACTIN	**Human/ Mouse**	**Forward (FW)**	**AATGTGGCCGAGGACTTTGAT**
β-ACTIN	**Human/ Mouse**	**Reverse (RW)**	**AGGATGGCAAGGGACTTCCTG**

seeding density in astrocyte medium on Geltrex-coated plates, following 5–10 min incubation with accutase (Thermo Fisher A1110501). Mature astrocytes were used after 30 days of differentiation, as described previously [13].

2.4. Mouse astrocytes isolation

Primary cultures of cortical astrocytes from mouse brains were generated following a modified version of a previously described protocol [14] under the protocol #ID 426/2024-PR of the Italian Ministry of Health. Briefly, neonatal mice (1–2 days old) were euthanized, and their brains were extracted under sterile conditions before being placed in phosphate-buffered saline (PBS) supplemented with calcium and magnesium (PBS-w; Aurogene, Rome, Italy; AU-L0625-500), along with antibiotics (100 IU/ml penicillin and 100 μg/ml streptomycin; Aurogene, AU-L0022-100). Using a stereomicroscope, the meninges were meticulously removed, and the cortical tissue was isolated. The dissected tissue was fragmented into small pieces and subjected to enzymatic digestion with trypsin in PBS lacking calcium and magnesium (PBS-w/o, Aurogene, AU-L0615-500) for 25 min at 37 °C. This digestion was followed by a 5-min incubation with DNAse I (Sigma Aldrich, D4513). Subsequently, the tissue was mechanically dissociated DMEM with high glucose (Aurogene, AU-L0103-500), supplemented with 10 % fetal bovine serum (FBS, Sigma Aldrich, F7524) and antibiotics (100 IU/ml penicillin and 100 μg/ml streptomycin; Aurogene, AU-L0022-100), to obtain a single-cell suspension. The isolated cells were then plated into 75-cm^2 flasks at a density of 1×10^7 cells per 10 ml (corresponding to one brain per flask) and maintained at 37 °C in a humidified incubator with 5 % CO_2. The culture medium was replaced after 24 h and subsequently renewed twice weekly. To eliminate contaminating microglial cells, astrocytes underwent two rounds of sub-culturing: the first in 75-cm^2 flasks and the second directly in multi-well plates for experimental applications. All experimental procedures were conducted in DMEM containing 1 % FBS and antibiotics. To validate the enrichment of astrocytes in our cell preparation, we performed a Western blot for GFAP, a well-established astrocytic marker. As shown in Supplementary Fig. S1, a markedly stronger GFAP signal is observed in the astrocyte-enriched preparation compared to total brain extracts, confirming a substantial enrichment of this cell type. To obtain total brain extract from the all brain of C57BL/6 mice were prepared in RIPA buffer (pH = 7.4) containing 50 mM Tris-HCl (pH = 8), 150 mM NaCl, 1 % NP-40, 0.5 % sodium deoxycholate, 1 mM EDTA, 0.1 % SDS, together with phosphatase and protease inhibitor (539,132, Millipore, 1:100; P0044; Sigma-Aldrich, St. Louis, MO, USA; 1:100). Samples were sonicated on ice and then centrifuged at 14.000 rpm at 4 °C for 30 min to remove cellular debris. Supernatants were collected to determine total protein concentrations by the BCA method (Pierce, thermofisher Scientific).

2.5. Western blot analysis

Approximately 350,000 cells were seeded per well in 6-well plates. The following day, cells were either left untreated or treated with specific inhibitors. BI605906, an IKKβ inhibitor (Sigma Aldrich), was applied at a concentration of 20 μM for 231BrM and 4T1BrM cell lines, and at 6 μM for the E0771BrM line. SU-909, an IKKα inhibitor (DC Chemicals, Shanghai, China), was used at a concentration of 8 μM for all three BrM cell lines (231BrM, 4T1BrM, and E0771BrM). Cells were harvested and total protein extracts were prepared in RIPA buffers (pH = 7.4) containing 50 mM Tris-HCl (pH = 8), 150 mM NaCl, 1 % NP-40, 0.5 % sodium deoxycholate, 1 mM EDTA, 0.1 % SDS (539,132, Millipore, 1:100; P0044; Sigma-Aldrich, 1:100). Protein concentration was determined using the Pierce BCA Protein Assay Kit (23,225; Thermo Fisher Scientific). 15 μg of proteins were separated by 4–12 % gradient SDS- electrophoresis using NuPAGE 4–12 % Bis-Tris-Gel (NP0323BOX; Invitrogen by Thermo Fisher Scientific) in MOPS SDS Running Buffer 20x (NP0001; Invitrogen). The proteins were then transferred onto nitrocellulose membranes and incubated overnight at 4 °C with the primary antibody: *anti*-IKKα (dilution 1:1000 D3W6N; Cell Signaling Cell Signaling Technology, Inc., MA, USA), *anti*-IKKβ (dilution 1:1000, D30C6; Cell Signaling), anti- IκBα (dilution 1:1000, L35A5; Cell Signaling), *anti*-TRAF6BP/TAX1BP1 (dilution 1:1000 A305645; Antibodies.com Ltd., Cambridge, UK), *anti*-β-Actin (4D3) (dilution 1:5000, A28272 anti-mouse; Antibodies.com), *anti*-EAAT1 Polyclonal antibody (dilution 1:1000, bs-1003R, Bioss Inc., MA, USA), *anti*-EAAT2 (E−1) (dilution 1:800, sc-3656,334; Santa Cruz Biotechnology, Inc., TX, USA) *anti*-GFAP (Glial Fibrillary Acidic Protein, 840,001, dilution 1:10,000 Biolegend San Diego, CA USA). Subsequently, membranes were incubated at room temperature with the respective horseradish peroxidase-conjugated secondary antibodies for 1 h: anti-mouse IgG, HRP linked antibody (dilution 1:2000, 7076P2; Cell Signaling), anti rabbit IgG HRP linked antibody (dilution 1:2000, 7074P2; Cell Signaling). Membranes were washed with TBS- 0.1 % Tween 20 and developed with Clarity enhanced chemiluminescence (ECL) substrate (Bio-Rad, Hercules, CA, USA, #1705061) and then acquired with Chemi-Doc MP (Bio-Rad, Hercules, CA, USA). The relative abundance of each protein was calculated using Image Lab 6.0.1 software (Bio-Rad Laboratories). Densitometric analysis was performed using Image Lab 6.0.1 software (Bio-Rad Laboratories).

2.6. Luciferase reporter assay

Cells were seeded at a density of approximately 350,000 per well in 6-well plates. and transfected with the jetPRIME transfection reagent (101000027; Life Sciences, Inc., CA, USA) for 24 h using a 0.5 μM NF-κB plasmid containing a luciferase reporter gene (Stratagene, now Agilent, CA, USA) [15], along with a 0.3 μM plasmid encoding Renilla luciferase [16]. Twenty-four hours later, treatments were carried out using specific pathway inhibitors for 5 h. The IKKβ inhibitor BI605906 (Sigma Aldrich) was administered at 20 μM for the 231BrM and 4T1BrM cell lines, while a lower concentration of 6 μM was used for E0771BrM. In parallel, the IKKα inhibitor SU-909 (DC Chemicals, Shanghai, China) was applied at 8 μM across all three BrM models. The experiment proceeded according to the Dual-Luciferase Reporter Assay System protocol (E1910; Promega Corporation, WI, USA). NF-κB activity for each sample was quantified by measuring the luminescence with the SpectraMax mini instrument, following the manufacturer's instructions, in brief, Firefly luciferase activity was measured by adding 100 μL of LAR II to the lysate, waiting 2 s, and reading luminescence for 10 s. Then, 100 μL of Stop & Glo® Reagent was added to quench Firefly and activate Renilla luciferase, followed by another 2-s wait and a 10-s luminescence reading. The obtained data were analyzed by calculating the ratio of the luminescent signal emitted by NF-κB activity to the signal emitted by Renilla luciferase. All experiments were performed with at least three technical replicates and independently repeated at least three times.

2.7. Cell migration

Cell migration assays were performed using 8.0 μm pore size inserts (662,638; Greiner Bio-One International GmbH, Kremsmünster, Austria). A total of 50×10^3 cells were resuspended in serum-free RPMI and seeded into the upper chamber of the insert. Serum-free RPMI was added to the lower chamber to establish the migration gradient. Cells were treated with or without IKKβ inhibitor at 20 μM for 231BrM and 4T1BrM cell lines, and 6 μM for the E0771BrM line. Additional conditions included treatment with L-glutamic acid monosodium salt (J63424, ThermoScientific) at 100 μM and DLTBOA at 50 μM. The chambers were then incubated for 8 h at 37 °C under 5 % CO_2. The supernatant was removed from the chamber and the non-migrating cells from the upper surface of the filter were removed by using a cotton swab. The cells were then stained with 0.1 % crystal violet for 10 min and washed with MilliQ water to remove the crystal violet excess. Cells

on the lower surface of the membrane were quantified by counting the stained cells that migrated to the lower side of the insert using an optical microscope EVOS XL CORE AMEX1000 (Invitrogen). Each experiment was performed with at least three technical replicates and independently repeated at least three times. Stained cells were counted as the mean number of cells per 6 random fields for each technical replicate.

2.8. Cell invasion

The invasion assay was performed using an 8.0 μm pore-size insert (662,638; Greiner Bio-One International GmbH, Kremsmünster, Austria). HCMEC/D3 cells (45,000 cells/well) were seeded in the insert and cultured for 2 days to form a monolayer. A total of 5 × 10^4231 BrM cells were resuspended in serum-free RPMI and seeded into the upper chamber of the insert. Serum-free RPMI or serum-free RPMI enriched with 100 μM total glutamate was added to the lower chamber, and the plates were incubated for 12 h at 37 °C under 5 % CO2. After incubation, the supernatant was discarded, and non-migrating cells on the upper surface of the filter were gently removed with a cotton swab. The cells that had migrated to the lower surface of the membrane were stained with 0.1 % crystal violet for 10 min, rinsed with MilliQ water to remove excess stain, and counted under an EVOS XL CORE AMEX1000 (Invitrogen) optical microscope. Each experiment was performed with at least three technical replicates and independently repeated at least three times. Stained cells were counted as the mean number of cells per 6 random fields for each technical replicate.

2.9. Seahorse XF analyzer respiratory assay

The extracellular flux Analyzer XFe96 (Seahorse Bioscience, Houston, TX, USA) was used to test the metabolic flexibility in different cell lines by measuring the mitochondrial oxygen consumption rate (OCR) indicator of oxidative phosphorylation, and extracellular acidification rate (ECAR) indicator of glycolysis rates using XF Cell Mito Stress Test (Agilent, CA; USA). The cells were cultured on XFe96 culture mini plates for a final density for the day of the assay of 3 × 10^4 cells/well and treated overnight as specified in the Treatment section. To ensure optimal cell density on the day of the experiment, cells were seeded using a proliferation correction factor based on their estimated growth rates: 1.66 × for 231, 1.7 × for 231-BrM, 2 × for 4T1 and 4T1-BrM, and 1.5 × for E0771 and E0771-BrM cells. The day after, the media were removed and replaced with or without each indicated treatment. DLTBOA treatment at 100 μM (1223; Tocris) for 231, 4T1, E0771, 231BrM, 4T1BrM and E0771BrM cell lines. IKKβ Inhibitor treatment (BI605906; Sigma Aldrich) at 20 μM for 231BrM, 4T1BrM and E0771BrM cell lines. Navarixin treatment (SCH- 527123; Selleckchem) at 15 μM for 231BrM, 4T1BrM and E0771BrM cell lines.

One day prior to the analysis, the XFe analyzer cartridge was hydrated at 37 °C in a non-CO_2 incubator. Before the assay, the XF-base Dulbecco's modified Eagle medium (XF-DMEM) was supplemented with 10 mM glucose, 10 mM pyruvate and 2 mM L-glutamine and then adjusted at pH 7.4. The cells were subsequently washed by and supplemented with 180 μl of XF-DMEM and then incubated for 60 min at 37 °C in a non-CO_2 incubator for gas equilibration. During the metabolic analysis, the cells were subjected to subsequent drug supplementation such as oligomycin (1 μmol/L) that inhibits ATP synthase, carbonyl cyanide p-trifluoromethoxy phenylhydrazone FCCP (1 μmol/L) that induces maximal uncoupled respiration and finally rotenone and antimycin A (0.5 μmol/L) in order to determine the non-mitochondrial respiration. OCR and ECAR were normalized for total protein/well. The optimal oligomycin/FCCP drug concentrations and cell density were initially characterized in independent experiments. Seahorse assay data were normalized to the number of cells present at the time of the assay by including in the calculation the total protein content measured in each well. Protein quantification was performed using the Pierce BCA Protein Assay Kit (23,225, Thermo Scientific), following the manufacturer's instructions."

2.10. Trypan blue exclusion assay

The day after seeding 350,000 cells in each well of a 6-well plate, cells were treated or not with varying concentrations of specific inhibitors. IKKβ inhibitor was applied at 0, 10, and 20 μM for the 231BrM and 4T1BrM cell lines, and at 0, 5, and 10 μM for E0771BrM. DLTBOA was administered at 0, 20, 50, and 100 μM across all cell lines, including 231, 4T1, E0771, 231BrM, 4T1BrM, and E0771BrM. Navarixin treatment was performed at 0, 5, 15, and 20 μM in the 231BrM, 4T1BrM, and E0771BrM cell lines. After the treatment period indicated in each figure the growth medium was collected, the cells were washed once with phosphate buffered saline (PBS-1A; Capricorn) and adherent cells were removed by treatment with trypsin (Trypsin-EDTA 0.25 % in HBSS 1X with phenol red; SIAL-TryEDTA), which was then blocked using complete medium. All the collected cell samples were combined with their corresponding supernatants, and the mixtures were centrifuged 5 min at 90 rcf. The supernatant carefully discarded. The harvested cells were then washed with PBS, centrifuged 5 min at 90 rcf and the supernatant discarded. Following the addition of a 0.4 % (w/v) trypan blue stain solution (EBT-001, NanoEntek Inc., Seoul, South Korea) cells were transferred to a cell counting slide (EVS-050, EveTM NanoEntek), visualized, and counted using EveTM Automatic Cell Counter, (NanoEntek). Cells stained with trypan blue dye were considered nonviable.

2.11. Cell permeability assay

HCMEC/D3 cells (45,000 cells/well) were seeded into 3 μm pore size inserts for 24 well plate (662,630; Greiner Bio) and cultured for 2 days to form a monolayer. Conditioned media from parental and metastatic cells (collected after 48 h) was then added to the top chamber of the inserts, HCMEC/D3 cells were treated or not with Navarixin (SCH- 527123; Selleckchem) at 15 μM for 231BrM, 4T1BrM E0771BrM, 231, 4T1, E0771 cells, RPMI-serum-free was added to the bottom chamber for 24 h. After 24 h, fluorescein isothiocyanate-dextran (46,945-100 mg; Sigma Aldrich) dissolved in PBS was added to the top chamber, and PBS to the bottom chamber for 2 h. Subsequently, the dextran from the upper chamber and PBS from the bottom chamber were collected. Dextran concentration was determined by measuring the absorbance at 495 nm at V-650 Spectrophotometer and calculated with Lambert-Beer law.

2.12. Glutamate uptake

iPSC-derived astrocytes, 231, 4T1, and E0771 cell lines and their respective BrM counterparts and were seeded and treated for 48 h with or without IKKβ Inhibitor (BI605906; Sigma Aldrich) at 20 μM; DLTBOA 80 μM (1223; Trocris) or Navarixin (SCH- 527123; Selleckchem) at 15 μM for 231BrM, 4T1BrM E0771BrM cell lines. Following the treatment, HBSS 1X (2026–08; GIBCO, Thermo Fisher Scientific Inc., MA, USA) was added for 10 min to equilibrate the cells. HBSS was then removed, and HBSS containing 200 μM L-glutamic acid monosodium salt (J63424, ThermoScientific) was added. Samples were collected at various time points. The glutamate uptake in each sample was quantified by measuring the absorbance at 450 nm using the Glutamate Assay Kit (MAK004; Sigma Aldrich) according to the manufacturer's instructions at the SpectraMaxmini instrument (Molecular Devices, San Jose, CA USA).

2.13. Elisa assay

The human IL-8 EH0205; FineTest Biotechnology Co., Ltd., Wuhan, China; GROα/Cxcl1, GROβ/Cxcl2 and GROγ/Cxcl3 ELISA assay kit human/mouse respectively (EH0005/EM0003, FineTest; EH3178/EM1090; FineTest, EH3179/EM1091; FineTest), were used to perform the ELISA assay. Conditioned media were collected from the plated cells

after 24h and applied to the ELISA plate, following the manufacturer's instructions. The final results were quantified by measuring absorbance at 450 nm using the SpectraMax mini-instrument. Cytokine concentrations in pg/μg for each sample were determined using the curve-fitting software provided in the protocol. IL-8, GROα, GROβ and GROϒ concentrations were normalized to cellular protein levels based on results obtained from the Pierce BCA Protein Assay Kit (23,225; Thermo Fisher Scientific).

2.14. Cytokine array

Conditioned cell media was collected after 48 h and added to C-Series Human Cytokine Antibody Array C5 membranes (AAH-CYT-5-8; RayBiotech, Inc., GA, USA) containing different antibodies for cytokine recognition. The experiment was performed according to the manufacturer's protocol, and cytokine expression was measured and acquired with Chemi-Doc MP (Bio-Rad, Hercules, CA, USA). The relative abundance of each cytokine expression was calculated using Image Lab 6.0.1 software. Here a complete list of the cytokines in the arrayI-309 (CCL1), IL-1 alpha (IL-1 F1), IL-1 beta (IL-1 F2), IL-2, IL-3, IL-4, IL-5, ENA-78 (CXCL5), G-CSF, GM-CSF, GRO alpha (CXCL1), IL-12 p40/p70, IL-13, IL-15, IFN-gamma, MCP-1 (CCL2), MCP-2 (CCL8), MCP-3 (CCL7), IL-6, IL-7, IL-8 (CXCL8), MIG (CXCL9), MIP-1 delta, RANTES (CCL5), SCF, SDF-1 alpha, TARC (CCL17), TGF beta 1, TNF alpha, M-CSF, MDC (CCL22), MIP-1 beta (CCL4), OSM, TPO, VEGF-A, PDGF-BB, Leptin, BDNF, TNF beta (TNFSF1B), EGF, IGF-1, Angiogenin, FGF-4, FGF-6, FGF-7 (KGF), FGF-9, FLT-3 Ligand, Fractalkine (CX3CL1), LIGHT (TNFSF14), GCP-2 (CXCL6), Eotaxin-1 (CCL11), Eotaxin-2 (CCL24), Eotaxin-3 (CCL26), IGFBP-3, IL-16, IP-10 (CXCL10), LIF, MCP-4 (CCL13), GDNF, HGF, IGFBP-1, IGFBP-2, NT-4, OPN (SPP1), OPG (TNFRSF11), PARC, PLGF, TGF beta 2, TGF beta 3, MIF, MIP-3 alpha, NAP-2 (CXCL7), TIMP-1, TIMP-2.

2.15. Immunofluorescence

Brains were collected from mice injected with 231 BrM cells and treated with PBS/DMSO. For further details, see the *In Vivo Experiments* section. Collected brains were frozen on a temperature-controlled freezing stage, coronal sectioned (30 μm) on a sliding cryostat (Leica Biosystems, Wetzlar, Germany). Brain sections were mounted on glass slide. Once dried, the sections were fixed with 4 % paraformaldehyde for 20 min at room temperature and washed three times with filtered PBS. Then, the slides were blocked with a filtered solution containing 10 % normal goat serum and 0.3 % Triton X-100 in TBS. The slides were incubated overnight at 4 °C with *anti*-GFAP (rabbit 1:200) antibody (BioLegend Inc, CA, USA). Slides were then washed with PBS and incubated with Alexa Fluor −594nm secondary antibody (Invitrogen Corporation, Carlsbad, CA, USA) at 1:1000 for 2h at room temperature. To keep the background in check, slices were stained with Sudan Black B (Sigma-Aldrich) 70 % ethanol solution for 20 min at room temperature, and then washed with PBS. All sections were incubated with 4′,6-diamidino-2-phenylindole (DAPI Staining kit, Cohesion Biosciences) (10 mg/ml) for 5 min. At the end cover slip glasses were placed using a drop of Fluoromount aqueous mounting medium (Sigma-Aldrich, St Louis, MO, USA). Images were acquired using a ZEISS AXIO microscope equipped with a 20 × objective (LD A-Plan 20 × /0.35 Ph1). For GFAP-Alexa Fluor 594, images were acquired with an Axiocam 503 camera using an exposure time of 10 s and binning mode 3 × 3; acquisition parameters were kept constant across experimental groups. For DAPI, images were acquired with an exposure time of 222.2 ms and the same binning mode (3 × 3); acquisition settings were likewise kept constant across samples. All images were captured at a resolution of 640 × 484 pixels using ZEN software, with an approximate field size of 200 μm × 200 μm.

2.16. Cytometric analysis

After a wash with PBS cells were detached by treatment with trypsin (Trypsin-EDTA 0.25 % in HBSS 1X with phenol red; SIAL-TryEDTA), which was then blocked using complete medium. Cells were harvested, washed in PBS, and centrifuged for 5 min at 90 RCF. Next, 300,000 cells were resuspended in 50 μL of PBS containing 5 μL of the appropriate antibody per million cells (following the manufacturer instructions) and incubated for 30 min. After incubation, the cells were washed with 1 ml of PBS, centrifuged, and the supernatant was discarded. The pellet was then resuspended in 300 μL of complete medium. Fluorescence emission was measured using a NovoCyte 1040 flow cytometer (Agilent). The following antibodies were used: PE anti-human CXCR2 (320,705, BioLegend, Inc., CA, USA) and APC anti-mouse CXCR2 (149,613, BioLegend).

2.17. Bionformatic analysis

A previously published dataset (GSE99394) was analyzed to compare the transcriptomes of circulating tumor cells (CTCs) from breast cancer patients with brain metastases to those from patients without brain metastases. Differential gene expression analysis was conducted using a custom R script (available upon request), utilizing the packages BiocManager, GEOquery, limma, and hta20transcriptcluster.db. The primary statistical test was the limma moderated *t*-test with Empirical Bayes moderation, applied to microarray data to identify genes differentially expressed between the two conditions (BCBM vs. No_BCBM). This procedure is optimized for high-dimensional data (e.g., thousands of genes) and small sample sizes.

2.18. In vivo experiments

All animal experiments were carried out under the authorization n° 312/2021-PR (prot. A69A0.87) of the Italian Ministry of Health. Thirteen 7-week-old female immunocompromised NOD. CB17 Prkdcscid IL2rgtm1/BcgenHsd mice (average weight 21 g) were purchased from ENVIGO (Udine, Italy). Mice were housed under standard laboratory conditions with a 12-h light/dark cycle, ambient temperature of 20–22 °C, and relative humidity of 40–60 %. Food and water were provided ad libitum. Environmental enrichment (e.g., nesting material) was included, and cages were cleaned regularly according to facility protocols. Immunocompromised mice were inoculated with 231BrM cells (2x105) via the carotid artery as previously described [17] and monitored for brain metastasis development using IVIS imaging. The mice were divided into two groups: one treated subcutaneously with iEAAT1/2 20 mg/kg in 100 μl PBS for five days a week and the control group treated subcutaneously with PBS/DMSO(8 %) 100 μl [18]. The 231BrM cells were stably transfected with the luciferase gene, enabling metastasis tracking through subcutaneous luciferin administration (1 mg/kg) and IVIS imaging. Metastasis growth was assessed after 7 and 15 days. All *in vivo* experiments were conducted at the PLAISANT S.R.L. animal facility (Rome, Italy). The data analysis from the IVIS system was conducted using AURA software.

Table 2
Summary of inhibitors used in this study.

Compound	Abbreviation	Target/Description
DLTBOA	iEAAT1/2	Inhibitor of EAAT1 and EAAT2 (glutamate transporters)
Navarixin	iCXCR1/2	Inhibitor of CXCR1 and CXCR2 (chemokine receptors)
BI-605906	iIKKβ	Inhibitor of IKKβ (IKK beta)
SU-909	iIKKα	Inhibitor of IKKα (IKK alpha)

2.19. Inhibitor handling and control conditions

IKKβ, IKKα, EAAT1/2, and CXCR1/2 inhibitors (see Table 2) are resuspended in 100 % DMSO. In each experiment, the control condition is treated with the same amount of DMSO as present in the highest inhibitor concentration, ensuring that the final DMSO concentration in the medium matches the highest volume derived from any inhibitor stock solution. This guarantees that any observed effects are due to the inhibitors themselves and not to DMSO exposure. The DMSO concentration in the cell culture medium never exceeds 0.6 % of the total volume. In *in vivo* experiments, the estimated DMSO concentration in the bloodstream of each animal is approximately 0.5 % of the total blood volume.

2.20. Transfection

2.20.1. Cell migration assay, seahorse XF analyzer respiratory assay, ELISA, and western blot analysis

For siRNA-based experiments, 231BrM cells were transfected with 25 nM siRNA targeting IKKβ (Gene symbol: *IKBKB*, sequence: CTGGAGAAGTACAGCGAGCAA) or with a non-targeting control siRNA (scrambled sequence: CAGGGTATCGACGATTACAAA), using siRNA premix reagents according to the manufacturer's instructions. Transfections were performed at the time of seeding, by plating approximately 300,000 cells per well in 6-well plates in complete growth medium. After 24 h, cells were harvested and either reseeded onto Seahorse XF assay plates, onto migration assay inserts (8 μm pore size), or maintained for an additional 24 h if intended for Western blot analysis. For plasmid-based experiments, cells were transfected at the time of seeding (approximately 300,000 cells per well in 6-well plates) using 1.5 μg of DNA per well. The following constructs were used: control plasmid (pcDNA3.1), IKKβ-dominant negative, and wild-type IKKα were kindly provided by Prof. Tuosto, Sapienza University [19]. Transfections were carried out using JetPrime reagent (Polyplus-transfection, Illkirch, France), following the manufacturer's protocol. For Western blot analysis, the transfection reaction was allowed to proceed for 48 h before protein extraction. After incubation, cells were washed with PBS and lysed for protein collection. For ELISA assays, cells were transfected as described above and, 24 h later, the medium was replaced with serum-free medium. Supernatants were collected at 24, 48 and 72 h post-transfection and assessed by ELISA for IL-8. The ELISA assay was normalized to cell number by measuring total protein concentration in each sample using the Pierce BCA Protein Assay Kit (Thermo Fisher Scientific). Time zero was defined as the point at which serum-free medium was added.

2.21. Statistical analysis

All data are presented as the mean ± standard deviation, except where otherwise specified in the Figure legends. The results are based on at least three independent biological experiments. Statistical analyses were performed using one-way ANOVA followed by Bonferroni post-hoc test for multiple comparisons. A p-value <0.05 was considered statistically significant. All p-values corresponding to the various histograms are reported in the respective figures. The statistical analysis for the bioinformatics data shown in Fig. 2F and G was performed using the moderated *t*-test from the limma package, which applies Empirical Bayes moderation. This approach is specifically designed for high-dimensional data (e.g., thousands of genes) and small sample sizes. For Fig. 6D, e and f a Mann–Whitney *U* test (Wilcoxon rank-sum) with continuity correction was performed to compare signal emission between the CTR and iEAAT1/2 groups at each time point, as data did not meet normality assumptions.

3. Results

3.1. Increased IKKβ and reduced IKKα drive constitutive NF-κB activation in BrM breast cancer cell lines

It has been previously observed that, with respect to 231 and 4TI triple negative breast cancer parental cell lines, the derivative brain seeking (BrM) cells 231BrM and 4TIBrM exhibit an extraordinarily high level of active NF-κB, suggesting a role for this pathway in the resistance mechanism to apoptosis, which also manifests as resistance to various chemotherapeutic drugs [20]. To broaden the scope of cell models for this study, we sought to assess NF-κB pathway activity in both the parental E0771 breast carcinoma cell line and its brain-seeking derivative, E0771BrM. To measure NF-κB activity we employed a luciferase/reporter assay as previously reported [15]. The results revealed that the E0771BrM cell line exhibits a marked increase in basal NF-κB pathway activation relative to the parental line, with luminescence values increasing from approximately 2 to 8 arbitrary units (a ~300 % increase), aligning with findings from 231BrM and 4TIBrM previously reported. Additionally, we performed the same assay on the 4TI and 4TIBrM pair, where we observed an even more pronounced induction of NF-κB activity, with values rising from about 10 to 200 arbitrary units (~1900 % increase) (Fig. 1A). Despite the previously published data, the molecular mechanism leading to the increase on NF-κB activity has not yet been elucidated in any of the BrM cell lines. To understand the origin of these high levels of NF-κB activity in 231BrM, 4TIBrM and E0771BrM, we conducted Western blot analysis of various components of the pathway. The data from Fig. 1B and Supplementary Fig. S2 reveal that in the 231BrM, 4TIBrM, and E0771BrM cells, the levels of the pathway inhibitor IκBα are reduced compared to each parental cell line by approximately 70 %, 50 %, and 30 %, respectively. A similar reduction is also observed in the TAX1BP1 levels in both 231BrM and E0771BrM cells of about 50 % and 20 % respectively. Interestingly, in 4TI BrM cells, TAX1BP1 levels are much lower compared to those in the other murine cell line E0771 and very similar or slightly higher with respect to those of the parental 4TI cells (Fig. 1B and Supplementary Fig. S2). These findings suggest that the primary cause of the increased NF-κB activity may be attributed to the reduced levels of both IκBα and/or TAX1BP1 inhibitors of the pathway. To enhance our understanding, we conducted Western blot analyses to evaluate the levels of other factors that typically regulate the stability of IκBα and the induction of TAX1BP1, specifically the kinases IKKα and IKKβ. Fig. 1C and Supplementary Fig. S3A indicate that IKKα is downregulated by approximately 35 % in 231BrM, 4TIBrM, and E0771BrM cells compared to their respective parental cells. On the other hand, IKKβ is found to be upregulated in 231BrM, 4TIBrM, and E0771BrM cells by approximately 300 %, 200 %, and 50 %, respectively, compared to their parental counterparts (Fig. 1C and Supplementary Fig. S3B). It is known that both IKKα and IKKβ kinases can induce the degradation of the inhibitor IκBα [21]. However, the relative levels presented in Fig. 1C suggest that IKKβ overexpression could induce the downregulation of IκBα in 231BrM, 4TIBrM and E0771BrM cells. To test this hypothesis, we inhibited IKKβ by treating 231BrM, 4TIBrM and E0771BrM cells with the specific inhibitor BI605906 (iIKKβ) [22], and then evaluated the levels of IκBα in treated and untreated cells. As hypothesized, treatment with the IKKβ inhibitor led to an upregulation of IκBα (Fig. 1D and Supplementary Fig. S3C), demonstrating that one of the functions of the elevated levels of IKKβ is to maintain low levels of IκBα, participating in the constitutive activation of NF-kB pathway in these cell lines. On the other hand, the reduced levels of IKKα in BrM cells suggest that, in this system, and especially in the parental cells, IKKα may be involved in the resolution of the inflammatory response, as previously reported [23]. To further validate this hypothesis, we targeted IKKα with the specific inhibitor SU-909 to evaluate the levels of TAX1BP1, since it is known that IKKα can regulate TAX1BP1 protein stability through autophagosomal degradation [24–26]. We used the parental 231 and E0771 cells, where the levels of

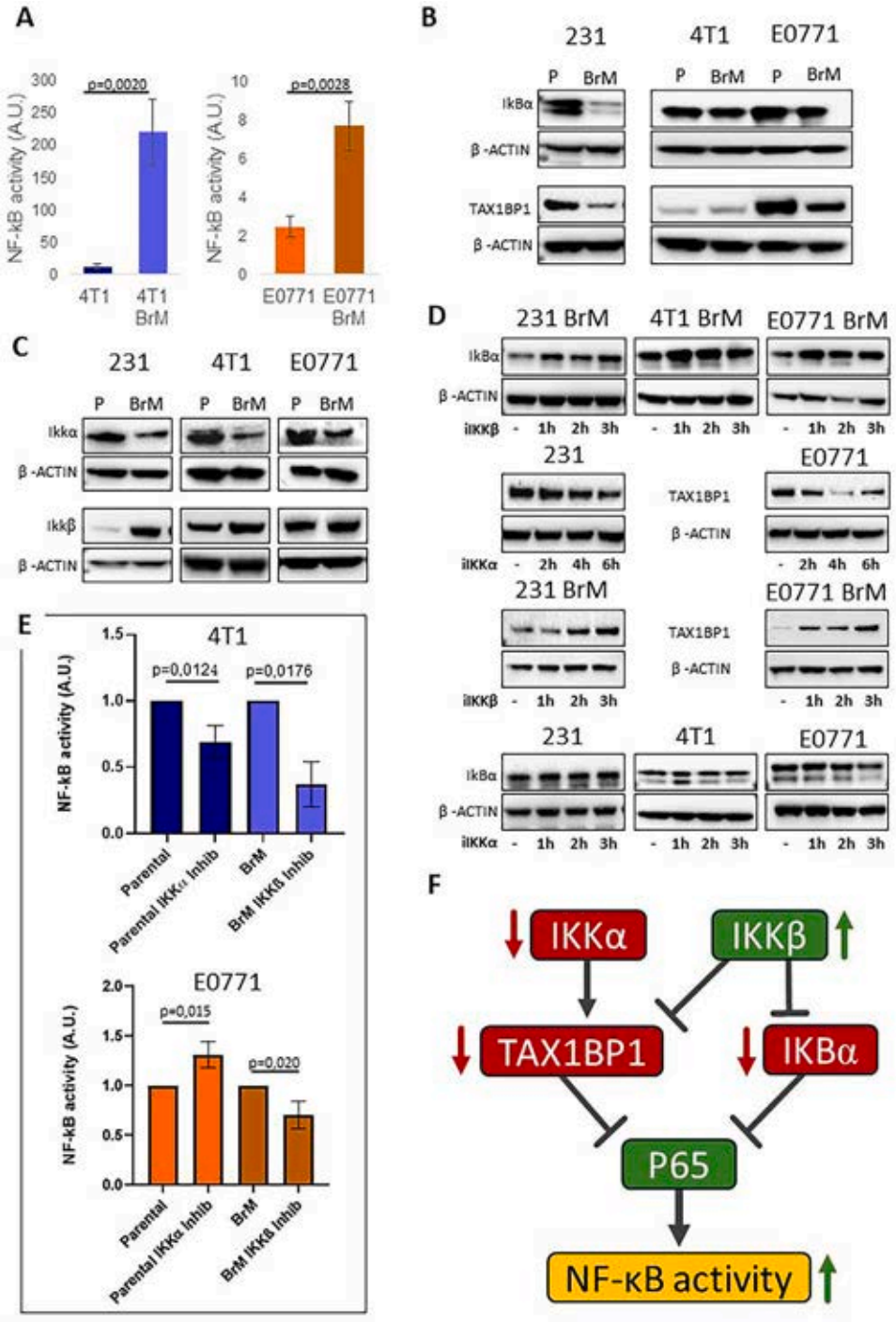

Fig. 1. IKKβ overexpression sustains constitutive NF-κB activation in brain-metastatic breast cancer cells through suppression of IκBα and TAX1BP1.
A and E: NF-κB activity was assessed in the specified cell lines using a luciferase reporter assay. In panel e, the IKKα inhibitor (iIKKα) was used at 8 μM, and the IKKβ inhibitor (iIKKβ) was used at 20 μM for 231BrM and 4T1BrM cell lines, and 6 μM for E0771BrM, both administered for 5 h; the p-value for each histogram is provided. B, C, and D: Western blot analyses were performed to evaluate the activation of the NF-κB pathway in the indicated cell lines using specific antibodies and inhibitors at the specified time points. The IKKα inhibitor (iIKKα) was used at 8 μM, and the IKKβ inhibitor (iIKKβ) was used at 20 μM for 231BrM and 4T1BrM cell lines, and 6 μM for E0771BrM; β-actin was used as loading control. F: Summary diagram illustrating how the pathway, with minor variations, operates in our model.

TAX1BP1 are high, while excluding the 4TI cells where the levels of this protein are lower. Fig. 1D and Supplementary Fig. S3D shows that treatment with IKKα inhibitor leads to a decrease in the levels of the inhibitor of NF-kB signaling TAX1BP1 in both 231 and E0771 cell lines of approximately 25 % and 30 % respectively. This clarifies why the 231BrM and E0771BrM cells exhibit a reduction in the levels of the kinase IKKα and a concurrent decrease in the levels of the NF-κB inhibitor TAX1BP1 [27]. To complete the study, we examined the role of IKKβ in regulating TAX1BP1 and of IKKα in controlling IκBα. We treated 231BrM and E0771BrM cells with an IKKβ inhibitor and assessed TAX1BP1 levels, observing that the treatment significantly reduced the levels of this protein (Fig. 1D and Supplementary Fig. S3E). The high variability in TAX1BP1 induction in E0771 cells following treatment with the IKKβ inhibitor may result from intrinsic heterogeneity in cellular responses or differential activation of compensatory pathways that modulate NF-κB feedback inhibition. The overall data confirm once again that IKKβ

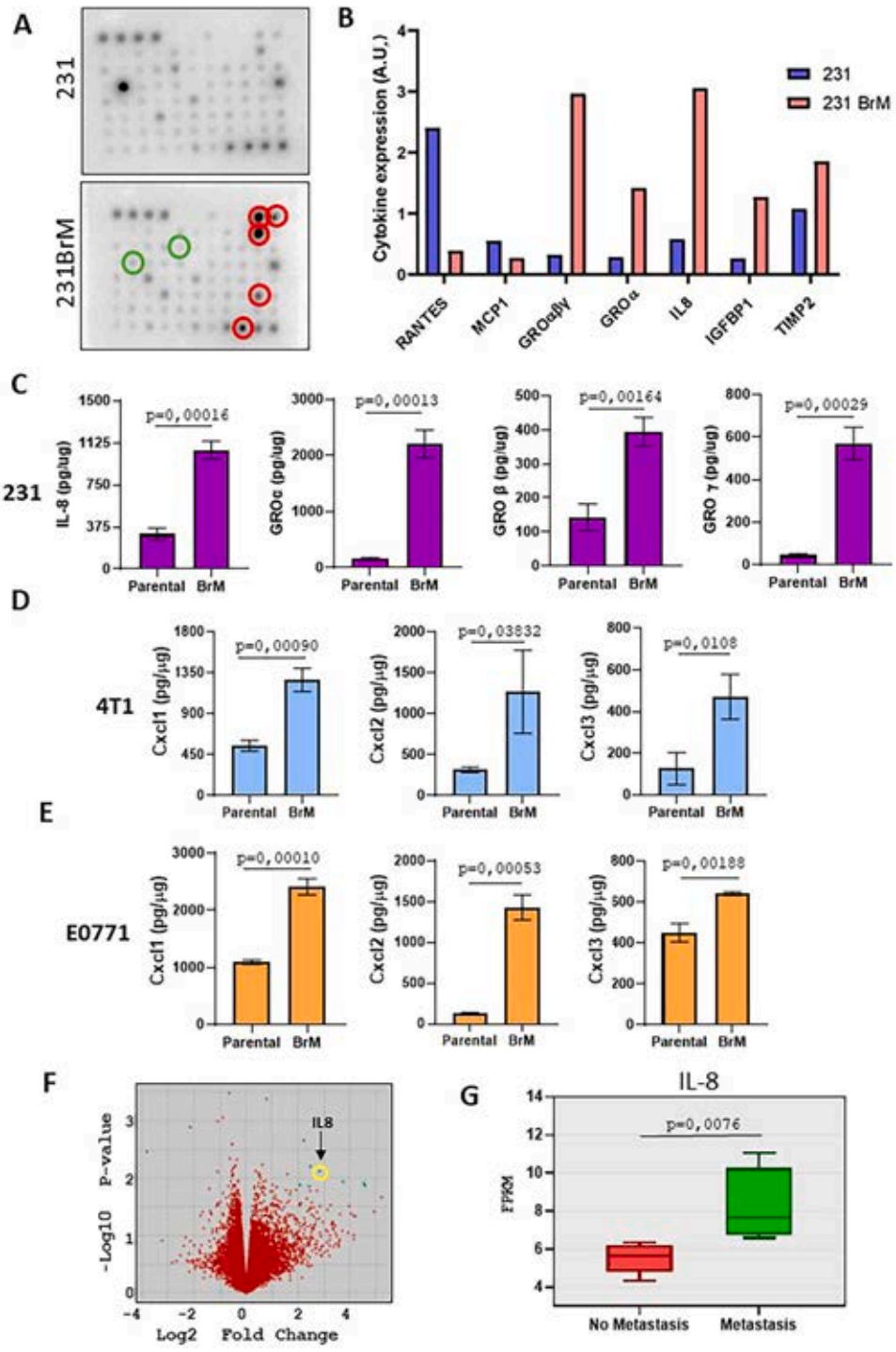

Fig. 2. brain-seeking breast cancer cells display a distinct cytokine secretion profile compared to parental cells.
A Cytokine array performed on conditioned media collected after 48 h from the indicated cell lines. Upregulated factors are marked in red, and downregulated factors in green, comparing 231BrM cells to their parental counterparts. B Densitometric analysis of the images shown in panel a. C, D, and E: quantification of the indicated cytokines in conditioned media collected after 48 h from the specified cell lines, measured using ELISA (pg/µg refers to the concentration of cytokine (in picograms) per microgram of cellular protein obtained trough BCA analysis). F: Volcano plot generated from data analysis of a database detailing gene expression in circulating tumor cells (CTCs) from breast cancer patients with and without brain metastases. G: quantification of IL-8 mRNA expression extracted from the analyzed database is shown in panel F. p value is reported for each of the histogram, for the statistical analysis see the specific section in materials and methods.

supports the constitutive NFκB signaling in BrM cells. In contrast, inhibition of IKKα in the parental cells had little to no effect on IκBα levels, indicating that this kinase likely plays only a minor role in regulating IκBα (Fig. 1D and Supplementary Fig. S3F). To validate the apparent constitutive inductive role of IKKβ and the inhibitory role of IKKα in our models, we employed the previously described NF-κB transcriptional activity gene reporter assay in both 4TI and E0771 cells, in the presence or absence of specific inhibitors for each kinase. Fig. 1E confirms that the IKKβ inhibitor reduces reporter activity in both 4TI BrM and E0771 BrM cell lines of about 65 % and 25 % respectively, while the IKKα inhibitor increases gene reporter activity in E0771 supporting our proposed hypothesis. In 4TI cells, treatment with the IKKα inhibitor also leads to a

reduction in NFκB activity, suggesting that, in these cells where TAX1BP1 is reduced, IKKα may maintain the function of support to the NF-kB signaling. Elucidating this function, however, is beyond the scope of this study. Overall, our data show that, although the role of IKKα may vary across different models, a common role for IKKβ was observed among the various cell lines examined. IKKβ functions as a powerful and constitutively active inducer of NF-kB signaling. Cells that metastasize to the brain clearly upregulate this gene to gain an advantage. A summary diagram of the key data related to the alterations in BrM cells compared to the parental cells is shown in Fig. 1F.

3.2. NF-κB-driven inflammatory reprogramming shapes a distinct cytokine profile

It is well-known that NF-kB is the master gene regulator of inflammatory processes, and that different settings of various pathway components can lead to the expression of different cytokine patterns [28]. To determine if the observed difference in expression of various pathway components between 231 and 231BrM, two of the best-characterized breast cancer and brain-metastatic models, could induce a distinct cytokine production pattern, we performed a cytokine array on the medium conditioned by these cells for 48 h. Fig. 2A reveals a markedly different cytokine pattern in the 231BrM cells conditioned medium compared to the parental 231, with at least 4 cytokines significantly upregulated and 2 distinctly downregulated among those tested. Densitometric analysis reveals that IL-8, GRO α, and GROα+β+γ exhibit the most significant levels of upregulation (Fig. 2B). Notably, these cytokines share a common pair of receptors highly related, suggesting them as particularly interesting target for further investigation in the context of our study. To validate these findings, we conducted ELISA experiments to assess the secreted levels of IL-8, and GROα, β and γ by both 231 and 231BrM cells. The data presented in Fig. 2C show that 231BrM cells produce approximately three times more IL-8 than 231 cells, 2.6 times more GRO-β, 6 times more GRO-γ, and about 20 times more GRO-α. To further investigate the causal relationship between IKKβ and IKKα expression and the activation mechanisms leading to cytokine production in our model, we used a plasmid encoding a dominant-negative form of IKKβ (IKKβ-DN) and another encoding the wild-type form of IKKα. While the ability of IKKα to form heterodimers with IKKβ and induce IκBα degradation has been extensively studied [29] the regulatory mechanism involving TAX1BP1 remains partially elusive. To clarify this pathway, 231BrM cells were transfected with a control plasmid (pcDNA3.1), the IKKβ-DN expression plasmid, or the wild-type IKKα expression plasmid. Supplementary Fig. S4A shows that both IKKβ-DN and IKKα overexpression lead to a marked increase in TAX1BP1 expression compared to control plasmid transfection suggesting an overall inhibitory effect exerted by both transfected factors. To better understand the biological effects on cytokine production induced by the modulation of IKKα and IKKβ in our model IL-8 expression was monitored in 231 BrM cells transfected with IKKα, IKKβ-DN, or the pcDNA3.1 control vector over a 72-h time course. At 24 h, cells expressing IKKα showed the highest IL-8 levels, indicating an early activation of the NF-κB pathway. However, IL-8 expression in these cells plateaued at 48 h and did not significantly increase thereafter. A similar pattern was observed in IKKβ-DN–transfected cells, which showed moderate IL-8 induction at 24 and 48 h, followed by stabilization through 72 h. By contrast, the control exhibited a steady, time-dependent increase in IL-8 expression, eventually surpassing both IKKα and IKKβ-DN by the 72-h time point (Supplementary Fig. S4B). These dynamics suggest that both IKKα-WT and IKKβ-DN modulate IL-8 induction in a temporally distinct manner compared to the unmodified control condition. To validate the data relative on cytokine expression on the two murine cell lines, we conducted ELISA experiments. Since IL-8 does not have a direct murine counterpart, we assessed the expression of Cxcl1 (the murine homolog of GROα), Cxcl2 (MIP-2, corresponding to GROβ), and Cxcl3 (equivalent to GROγ). The data presented in Fig. 2D and e shows that both 4TIBrM and E0771BrM cells secrete high levels of all the cytokines analyzed with respect to the parental counterpart. This supports the hypothesis that the alteration in the NF-KB pathway observed is reflected in common changes in the pattern of inflammatory cytokines released by cells with a common tropism for the brain. To assess how consistently cytokine secretion is associated with brain-metastasizing tumor cells, we re-analyzed a publicly available, previously published transcriptomic dataset. This dataset compares circulating tumor cells (CTCs) from breast cancer patients with brain metastases to those from patients without brain involvement [30]. Despite the limited number of patients enrolled (5 with brain metastasis and 5 without brain metastasis) in the reanalyzed study, at least four genes were found to be significantly differentially expressed between the two groups (Fig. 2F). Two of these genes are inflammatory cytokines, with IL-8 being the most overexpressed gene in the CTC from patients with brain metastases (Fig. 2F and G).

3.3. Inflammatory factors from BrM breast cancer cells drive endothelial barrier disruption and astrocyte activation

To investigate the biological effects induced by the cytokines released from BrM cells we performed *in vitro* and *in vivo* experiments. It is known that cancer cells in some contexts mimic immune cells in an attempt to trigger the opening of endothelial barrier through secreted inflammatory factors, and then invade the organ parenchyma which will subsequently be colonized [6]. To understand whether the inflammatory factors secreted by BrM cells are responsible for this specific phenomenon, we used the human BBB cell line HCMEC/D3. Interestingly, the inflammatory factors most highly secreted by our brain-seeking cells, namely IL-8 and GRO α, β, and γ, share the same receptor pair, CXCR1/CXCR2, which were previously found to be substantially expressed by HCMEC/D3 cells [31]. The HCMEC/D3 cells were seeded on a porous transwell filter and allowed time to form a barrier [31]. These cells were then treated with conditioned media from BrM cell lines and their respective parental cells for 24 h. Barrier permeability was subsequently assessed using a dextran assay previously described [32]. Fig. 3A demonstrates that all three types of BrMs cells are significantly more effective than the parental cells at inducing the permeabilization of the barrier formed by HCMEC/D3 cells. This results in an approximately 2-fold increase in permeability induction for the 3 cell lines. The specific inhibitor Navarixin (iCXCR1/2), which can block both CXCR1 and CXCR2 receptors, shared among the overexpressed cytokines [33], is able to reverse at the level of the parental cells the permeabilization process induced by the conditioned media alone from the 3 BrM cell lines (Fig. 3A). These data demonstrate that the process of permeabilization of HCMEC/D3 cells is mediated specifically by the cytokines overproduced by BrM cell lines. To demonstrate that factors secreted by brain-seeking cells play an active and effective role *in vivo*, we conducted histological analysis on metastatic brain tissue from mice injected with 231BrM cells via the carotid artery. As previously reported, inflammatory cytokine stimulation strongly increases GFAP expression in astrocytes *in vivo* [34]. Fig. 3B shows that the expression level of GFAP in the healthy tissue is very low, and this expression is also absent within areas identified as metastases by DAPI staining (blue), recognizable by the presence of tightly packed cell clusters. In contrast, GFAP expression (red) is abundant at the interface between metastatic and healthy tissue, suggesting astrocyte recruitment and/or activation likely triggered by inflammatory factors secreted by 231BrM cells in the microenvironment.

3.4. NF-kB-driven upregulation of EAAT1 and EAAT2 fosters a metabolic advantage in brain-metastatic breast cancer cells

The maintenance of membrane potential, neurotransmitter synthesis, and the triggering of postsynaptic potentials are some examples of the energy-intensive processes undertaken by neurons. To sustain their

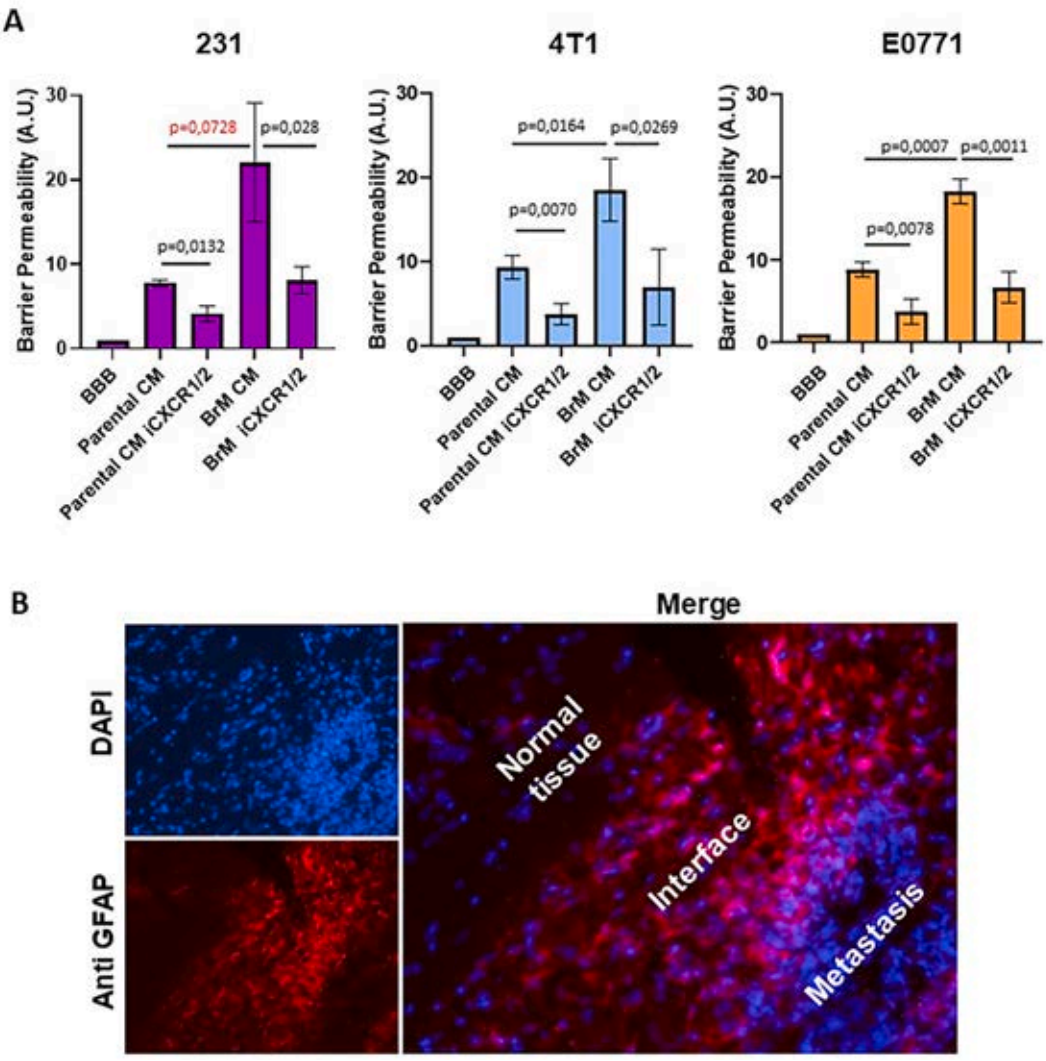

Fig. 3. Factors secreted from brain-seeking breast cancer cells increase BBB permeability and induce astrocyte activation.
A: Permeability assay performed on HCMEC/D3 cells using dextran. Prior to the assay, the cells were treated or left untreated (control) for 48 h with conditioned media from the indicated cell lines, in the presence or absence of the cytokine receptor inhibitor iCXCR1/2, used at a concentration of 15 μM. B: histological analysis of tumor masses form mice inoculated with 231 BrM cells, using an antibody against GFAP (red) and DAPI (blue). The different tissue types are indicated in the merged image.

high metabolic demands, neurons consume large amounts of glucose, partially limiting its availability for other cell types within the brain's extracellular environment [35]. It has been previously demonstrated that tumor cells invading brain parenchyma must utilize alternative energy sources, such as branched-chain amino acids or glutamine [35]. Considering the abundance and importance of glutamate in the interstitial fluid of the brain [7,36] as a potential energy and anabolic source, and the previously observed connection between glutamate transporters and inflammation in a completely different context [37], we explored a potential connection between the NF-kB pathway and the expression of glutamate transporters in our cancer model. We employed Western blot analysis to assess the levels of the glutamate transporters EAAT1 and EAAT2 in parental and brain seeking cell lines. Fig. 4A and Supplementary Fig. S5 show that 231BrM, 4TlBrM, and E0771BrM cells display increased levels of EAAT1 compared to their respective parental counterparts, with the highest induction observed in 231BrM cells, showing an approximately 30-fold increase. Intriguingly, we also observed, in the same comparison, elevated levels of EAAT2 (Fig. 4A and Supplementary Fig. S5) with the highest increase (approximately 2.2-fold) observed in E0771BrM cells relative to their parental counterpart. To understand if the increased expression of the EAAT1 and EAAT2 transporters in BrM lines could be induced by the increased NF-KB activity, particularly by the increased levels of IKKβ, we evaluated the expression of the two transporters after targeting of IKKβ, by treating the BrM cells with iIKKβ for 48 h. The data in Fig. 4B and Supplementary Fig. S5 show that the IKKβ inhibitor can reverse and reduce the heightened expression of both transporters in the all BrM cell lines by approximately 40 %–50 %, directly linking the alteration in NF-κB signaling to metabolic adaptations in glutamate utilization. Since it is known that inflammatory cytokines secreted by tumor cells can have an autocrine effect on the same cells that produce them, altering their behavior under various conditions [38], we aimed to study the involvement of CXCR1 and CXCR2 receptors in the mechanism of overexpression of the glutamate transporters EAAT1 and EAAT2 in our BrM lines. First, we sought to confirm the expression of CXCR1 and CXCR2 in our cells by quantitative real-time PCR. As shown in Supplementary Fig. S6, CXCR2 is generally the most highly expressed receptor of the two across the cell lines, except for 231 BrM, where the mRNA levels are comparable. Additionally, CXCR2 is the only truly functional receptor in mice [39]. We then used specific antibodies against CXCR2 and evaluated its expression through flow cytometry. Fig. 4C demonstrates that CXCR2 is expressed across all analyzed cell lines. Notably, 231 BrM exhibit higher protein expression

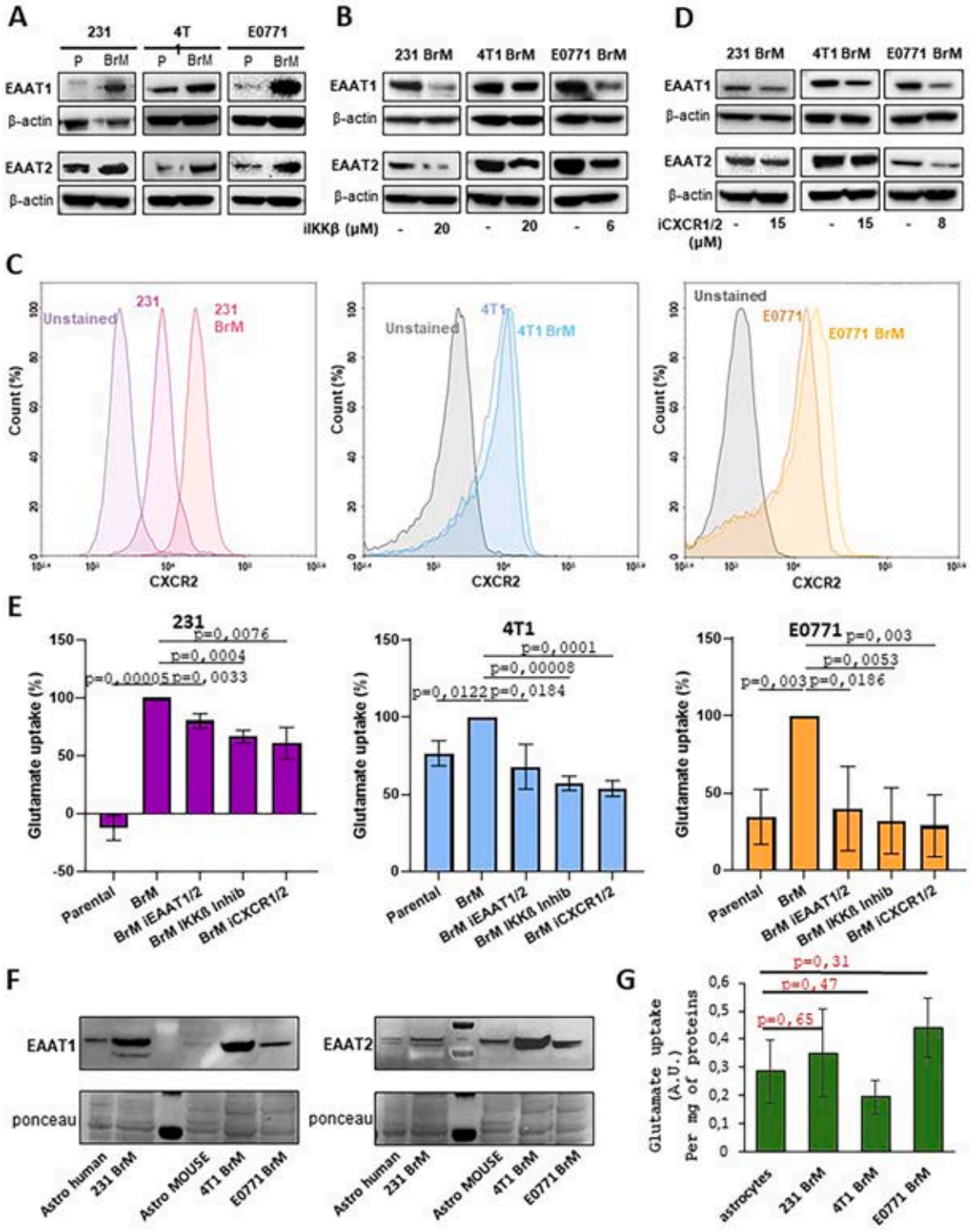

Fig. 4. Brain-seeking breast cancer cells overexpress glutamate transporters regulated by NF-κB and CXCR1/2 signaling, and increase glutamate uptake.
A, B, D and F: Western blot analysis was used to evaluate the expression of EAAT1 and EAAT2 transporters in the indicated cell lines or cells, in the presence or absence of the specified inhibitors at the indicated concentrations. Actin was used as a loading control. In C flow cytometric analysis was conducted to assess the expression of the CXCR2 receptor in the indicated cell lines. E NF-κB luciferase reporter assay performed on the specified cell lines treated or not with iCXCR1/2. In E and G glutamate uptake capacity was evaluated in the indicated cells using a specific kit (see materials and methods). The p values for each histogram are reported.

levels compared to the respective counterparts, whereas 4TI and E0771 parental and the relative BrM cells show comparable levels of receptor expression. The apparent discrepancy between the levels of CXCR2 expression in 231BrM cell measured by qRT-PCR and those observed by flow cytometry could potentially be explained by amplification at the translational level. Such mechanisms, like those mediated by the eukaryotic initiation factor eIF4E, are well-documented in inflammatory contexts [40]. However, clarifying this point will require further investigation. We then conducted Western blot experiments to evaluate the expression of EAAT1 and EAAT2 transporters in the presence or

absence of iCXCR1/2. Fig. 4D and Supplementary Fig. S5 shows that inhibition of these receptors partially reduces the expression of glutamate transporters, particularly EAAT1, in all three brain-seeking lines. The effect is less evident for EAAT2. This suggests a direct role of the secreted cytokines in supporting the signaling that could promote altered glutamate uptake in BrM cells. To validate the hypothesis that BrM cell lines utilize glutamate differently with respect to their parental cell line, we employed DLTBOA (iEAAT1/2), a specific inhibitor of the EAAT1 and EAAT2 transporters [41]. To begin with, we tested for any toxic effects of this compound on all the six cell lines. Supplementary Fig. S7 shows that iEAAT1/2 has minimal impact on cell viability, with a statistically significant toxic effect observed only at the 50 μM concentration in parental 4T1 cells. This suggests a potential role for the glutamate in supporting survival of this specific cell line. On the other hand, in 231 cells, a slight increase in cell viability is observed upon treatment with iEAAT1/2, suggesting a complex metabolic role of glutamate flux in these systems that warrants further investigation. To assess the glutamate uptake levels of the cell lines and the effectiveness of iEAAT1/2 in inhibiting this process, we conducted glutamate uptake assays using a specific kit in presence or not of iEAAT1/2. Fig. 4E shows that all BrM cell lines import higher levels of glutamate compared to their respective parental cells, by approximately 100 % in 231BrM, 20 % in 4TIBrM, and 70 % in E0771BrM, and that inhibition of EAAT1/2 partially reduces their glutamate uptake capacity. To validate the possible link between the upregulated NF-kB pathway of BrM cell lines with the activity of glutamate transporters, the previously described glutamate uptake experiments were conducted with and without treatment with the IKKβ inhibitor or CXCR1 and CXCR2 inhibitor iCXCR1/2. We first assessed the potential toxicity of the iIKKβ or iCXCR1/2 on our cells. Supplementary Fig. S8 and Supplementary Fig. S9 indicate that, while iIKKβ shows no signs of toxicity even at the highest doses after 48 h, the compound iCXCR1/2 induces mild toxic effects that reach statistical significance only in the 4T1-BrM cell line after 48 h. This suggests a possible role for inflammatory cytokines in supporting the survival of these specific cell line. Fig. 4E shows that both IKKβ inhibitor and iCXCR1/2 reduces the ability of all BrM cells to import glutamate, validating the close connection between the alteration of the inflammatory mechanism described in BrM cells and the preference of these cells for using this amino acid through uptake from the extracellular environment. To determine whether the amount of EAAT1/2 transporters and glutamate uptake activity in tumor cells makes them genuinely competitive compared to other highly specialized cells, such as astrocytes, we generated human astrocytes from pluripotent stem cells and isolated murine astrocytes from mouse brains. We then compared the expression levels of EAAT1/2 transporters and the glutamate uptake capacity between astrocytes and BrM tumor cells. Fig. 4F illustrates that glutamate transporter expression is significantly higher in BrM tumor cells when compared to astrocytes of the same origin. Specifically, 231 BrM cells exhibit remarkably high levels of EAAT1 compared to human pluripotent-derived astrocytes. Similarly, 4TI BrM cells express substantially higher levels of EAAT2 relative to murine astrocytes, while E0771 BrM cells show intermediate levels of both transporters, yet consistently higher than their murine astrocyte counterparts. To validate these expression data, we also compared the glutamate uptake activity between BrM cells and astrocytes. BrM cells demonstrated a glutamate uptake capacity comparable to that of astrocytes, which are highly specialized for glutamate reuptake (Fig. 4G). This strongly suggests the potential for competition between these two cell types.

3.5. *NF-κB–driven inflammatory signaling and glutamate-fueled metabolic reprogramming propel invasiveness of BrM breast cancer cells*

To further investigate the metabolic utilization of glutamate as a possible energy source by parental and BrM cells, we conducted Seahorse analysis to assess the energetic profile of both cell lines, with and without iEAAT1/2 treatment. Fig. 5A, B and C indicate that, compared to untreated cells, the parental cells exhibit only a very slight decrease in energetic metabolism in the presence of iEAAT1/2, primarily affecting mitochondrial respiration. In 4TI cells, this reduction is slightly more pronounced, affecting both OCR and ECAR, with a decrease of approximately 23 % and 15 %, respectively. In contrast, all the BrM cell lines treated with iEAAT1/2 exhibit a marked decrease in their energetic metabolism, both in terms of mitochondrial respiration and glycolysis, suggesting a greater utilization of glutamate in various aspects of cellular energy metabolism (Fig. 5A, B and C). The impact of inflammatory mechanisms on metabolism, especially in immune cells, has been thoroughly researched [42]. To understand the impact of the active inflammatory mechanism on the overall energetic metabolism in BrM cells, we conducted Seahorse experiments using IKKβ inhibitor also comparing the effects of this compound with those obtained using the glutamate transporter inhibitor (iEAAT1/2) mentioned above. Fig. 5A, B and C indicate that the inhibitory effect for respiration (only in 4TI) and glycolysis (in 231 and 4TI) induced by the IKKβ inhibitor significantly exceeds that of iEAAT1/2 alone, suggesting that the NF-kB pathway could have a broader influence on cellular metabolism, likely extending beyond just glutamate utilization. To validate our IKKβ findings, we also employed a genetic approach using an RNA interference targeting specifically IKKβ (IKKβ int.). As a preliminary experiment, we performed Western blot analysis to assess the efficiency of RNA interference. Supplementary Fig. S10A confirms a partial reduction of IKKβ protein levels (approximately 45 %) in 231BrM cells transfected with the IKKβ interference construct (IKKβ int.) compared to those transfected with the scrambled control sequence (Scr). This partial reduction is likely due to the inherently high baseline expression of IKKβ in 231BrM cells, which may limit the overall silencing efficiency. We then performed a new Seahorse analysis, comparing cells transfected with IKKβ interference to those transfected with the Scr control sequence. Both OCR and ECAR measurements showed reductions similar to those observed with the pharmacological inhibitor iIKKβ: OCR decreased by approximately 28.1 %, and ECAR decreased by approximately 25 % (Supplementary Fig. S10B). Considering the metabolic reprogramming that is particularly reliant on glutamate uptake in BrM cells, we aimed to evaluate whether this pathway is involved in the migratory processes underlying tumor cell invasiveness. We have previously demonstrated that extracellular amino acids, particularly serine and glycine, plays a fundamental role in the migratory capacity of metastatic cells and that these amino acids may have a role in tissue-specific invasion [9]. Glutamate is abundantly secreted into the extracellular fluid of the brain [7] and plays a critical role in the metabolism and survival of metastatic tumor cells [8]. To determine whether glutamate, by sustaining the energy metabolism of BrM cells, also influences their migratory ability and thus their capacity to invade brain parenchyma, we conducted migration assays on these cells in the presence of an increased amount of glutamate and/or the glutamate transporter inhibitor iEAAT1/2. As shown in Fig. 5D, an increased concentration of glutamate up to 100 μM in the culture medium significantly increase the migratory ability of all three BrM cell lines, with the effect being particularly pronounced in 231 BrM and 4TIBrM cell lines and slightly less evident in E0771 BrM. In all cell lines, however, the increased chemokinesis was inhibited in the presence of iEAAT1/2. To validate the importance of the altered inflammatory mechanism in BrM cells and its involvement in the migratory ability, we performed migration assays in the presence of an IKKβ inhibitor and an interference against IKKβ. As expected, we observed a dramatic reduction in the migratory ability of all our BrM cell lines following both pharmacological inhibition (Fig. 5E–F) and RNA interference (Fig. 5G). Specifically, migration was reduced by approximately 60 % in 231BrM cells and by about 75 % in both 4T1 and E0771BrM cells upon inhibitor treatment. Moreover, IKKβ silencing in 231BrM cells alone resulted in a ~55 % decrease in migration, confirming the key role of this pathway in sustaining the invasive behavior of brain-metastatic cells.

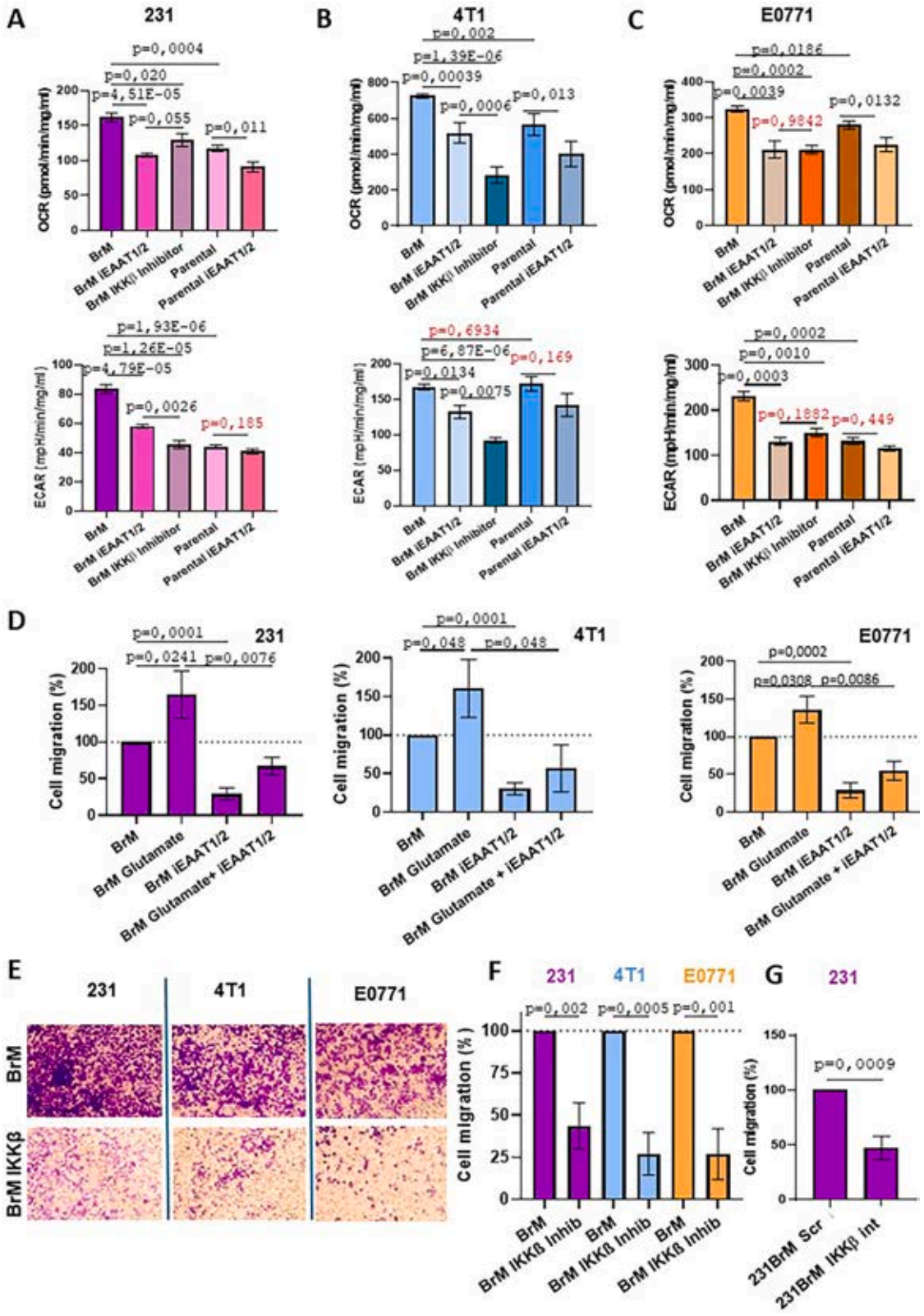

Fig. 5. NF-κB signaling and glutamate support metabolic activity and migration of brain-seeking breast cancer cells.
A, B, and C: Oxygen consumption rate (OCR) and extracellular acidification rate (ECAR) were measured using Seahorse analysis for the indicated cell lines. Cells were treated with iEAAT1/2 (100 μM) or an IKKβ inhibitor (20 μM) for 24 h prior to the analysis; Seahorse assay measurements were normalized to the cellular protein content of each well, determined via BCA assay. D: Cell migration assays were performed on the indicated cell lines, treated or untreated with iEAAT1/2, using transwell chambers. E (representative images) and f (mean results): Data from migration assays conducted over 8 h in the presence or absence of the IKKβ inhibitor, with a 2 h pretreatment. G: Migration assay performed for 8 h, 48 h after transfection with either control or IKKβ-targeting RNA interference sequences. p-values for each histogram are reported.

3.6. Pharmacological inhibition of glutamate uptake suppresses brain metastasis formation in vivo

To *in vivo* demonstrate the critical role of glutamate uptake and utilization in the process of brain metastasis formation, we conducted experiments inhibiting the glutamate uptake mechanism in 231BrM cells. As a preliminary *in vitro* experiment, we used a transwell system to mimic the microenvironment where extravasation takes place. We placed previously characterized [9] brain extracellular fluid (BEF) in the lower chamber and mouse serum in the upper chamber. We then monitored the migratory ability of 231 BrM cells in the presence or absence of iEAAT1/2, using the control medium alone as a negative control. Fig. 6A shows that the cells exhibit a markedly higher migration rate in the presence of BEF compared to the control medium, and that

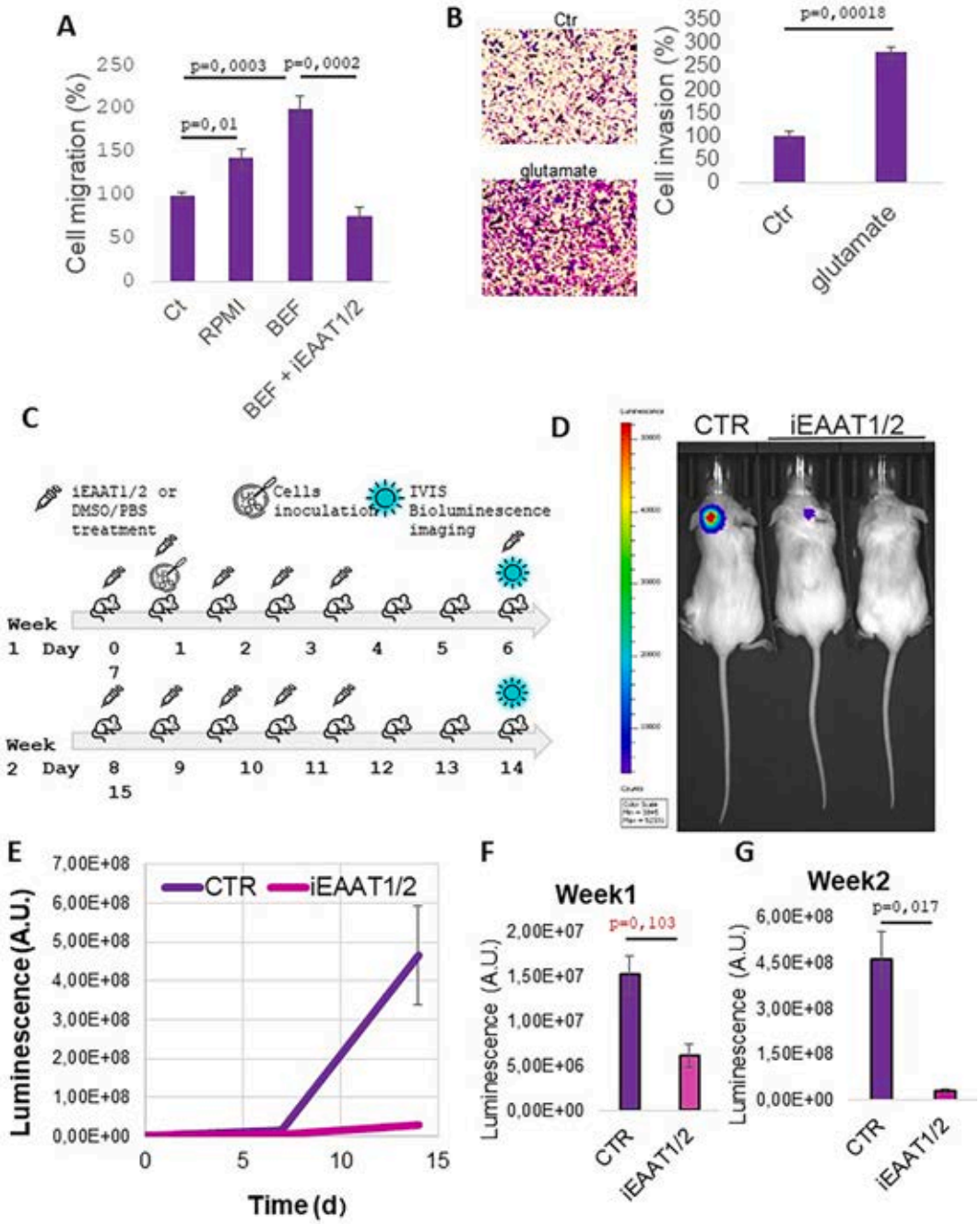

Fig. 6. Inhibition of glutamate transport reduces migration *in vitro* and brain metastasis formation *in vivo*.
A: preliminary migration assay was performed using a transwell chamber prepared as follows: (upper chamber/lower chamber) conditions included mouse serum/mouse serum (ctr), mouse serum/RPMI (RPMI), mouse serum/brain extracellular fluid (BEF), and mouse serum with iEAAT1/2/BEF (BEF + iEAAT1/2). B: Preliminary test showing a 24-h invasion assay of 231BrM cells through a HCMECD3 barrier, with the lower chamber containing either serum-free medium or medium supplemented with 100 μM glutamate. C: schematic representation of the experimental plan conducted *in vivo*. D: IVIS analysis is shown for mice injected and treated subcutaneously with either iEAAT1/2 (n = 7) or PBS/DMSO (control) (n = 5), following the protocol outlined in the scheme in panel C; The difference in the emission intensity scale between the two images is due to the automatic exposure optimization system used during image acquisition to best capture the light emission. Panels E, F, and G show graphical representations of luminescence emissions obtained through IVIS analysis (mean ± SEM) in mice inoculated with 231 BrM cells, comparing iEAAT1/2 and control groups at 1 and 2 weeks of treatment, a Mann–Whitney *U* test (Wilcoxon rank-sum) with continuity correction was performed to compare signal emission at each time point, as data did not meet normality assumptions. p-values for each histogram are reported.

their BEF-induced migration is inhibited in the presence of iEAAT1/2. As a further preliminary test, we aimed to confirm our cells' invasive capacity using a transwell system in which HMECD3 cells were seeded on the porous membrane to form a barrier that mimics the blood-brain barrier (BBB). We then placed a high-glutamate medium in the lower chamber and introduced the invading cells into the upper chamber. As shown in Fig. 6B the presence of glutamate led to a marked increase in the cells' invasive ability, with an approximately 2.5-fold induction. These preliminary findings underscore the crucial role of glutamate and its transporters in the mechanism of invasiveness. We then monitored the development of brain metastases in immunocompromised mice inoculated with 231BrM cells via the carotid artery. The mice were divided into two groups: one group was treated with 20 mg/kg iEAAT1/2 for five days a week, while the control group was treated with the same schedule with PBS/DMSO. The 231BrM cells inoculated were stably transfected with the luciferase gene, allowing us to track metastasis growth through luciferin administration and IVIS imaging. The mice were observed over a period of 15 days, with metastasis growth evaluated after 7 and 15 days (experimental plan in Fig. 6C). The data in Fig. 6D–F shows that mice treated with iEAAT1/2 exhibited a lower IVIS signal compared to PBS/DMSO-treated control mice. Although a decreasing trend was observed at 7 days post-inoculation (Fig. 6E–F), the difference was not statistically significant. However, after 15 days, the signal in iEAAT1/2-treated mice was almost 15-fold lower than in control mice, reaching statistical significance (Fig. 6E–G). This indicates that inhibiting glutamate uptake with iEAAT1/2 effectively limits the development of brain metastases.

4. Discussion

In this study, we demonstrate that BrM breast cancer cells acquire elevated NF-κB activity by downregulating IKKα and upregulating IKKβ, resulting in the constitutive activation of NF-κB. This sustained activation drives cytokine production, which, through the expression of the specific receptors CXCR1 and CXCR2 reinforces a positive feedback loop. Constitutively active NF-κB also induces the expression of the glutamate transporters EAAT1 and EAAT2, promoting glutamate uptake in BrM cells, where it serves as a metabolic fuel that enhances chemokinesis (Fig. 7). The high concentration of inflammatory cytokines in the tumor microenvironment further supports a pro-metastatic niche, probably facilitating the paracellular invasion of cancer cells through the blood–brain barrier (BBB). In vivo, inhibition of glutamate uptake significantly reduces brain metastases, underscoring the inflammatory–metabolic axis as a promising therapeutic target. We first aimed to clarify the origin of the constitutive NF-κB pathway activation previously observed in certain cell lines, such as 231BrM and 4TI BrM, compared to their parental cells [20]. Along with E0771BrM, which also exhibits high basal NF-κB activity relative to its parental E0771 line, these BrM variants preferentially form brain metastases when injected into both immunocompromised and syngeneic mice [11,12,43]. We demonstrated that this hyperactivation of NF-κB arises from two main changes: downregulation of the kinase IKKα and upregulation of the kinase IKKβ. This imbalance strongly suggests distinct roles for IKKβ (pro-tumoral) and IKKα (anti-tumoral under normal conditions), where IKKα also helps shut down inflammatory signals [27]. A similar imbalance has been investigated in gastrointestinal tumors, in which IKKα levels vary depending on the subtype, while IKKβ consistently shows upregulation compared to healthy tissue [44]. These findings, together with the data presented here, identify IKKβ as a particularly promising therapeutic target. Specifically, in all three BrM cell lines examined, IKKβ overexpression reduces IκBα and TAX1BP1 levels, two inhibitors of the NF-κB pathway [45]. In contrast, in parental 231 and E0771 cells, IKKα supports TAX1BP1 expression. Notably, the parental 4TI line represent an interesting model for dissecting this mechanism, as they exhibit significantly lower levels of TAX1BP1 compared to E0771 cells. This suggests that in 4TI cells, IKKα no longer relies on TAX1BP1 for its inhibitory function and instead supports NF-κB signaling without TAX1BP1's negative contribution. The inductive role of NF-κB via IKKα activation has been reported in other models as well [46]. Overall, our data indicate that constitutive NF-κB activation in BrM cells is likely due to an IKKα/IKKβ imbalance favoring IKKβ homodimers, which maintain continuous NF-κB signaling [47], in the absence of IKKα's negative

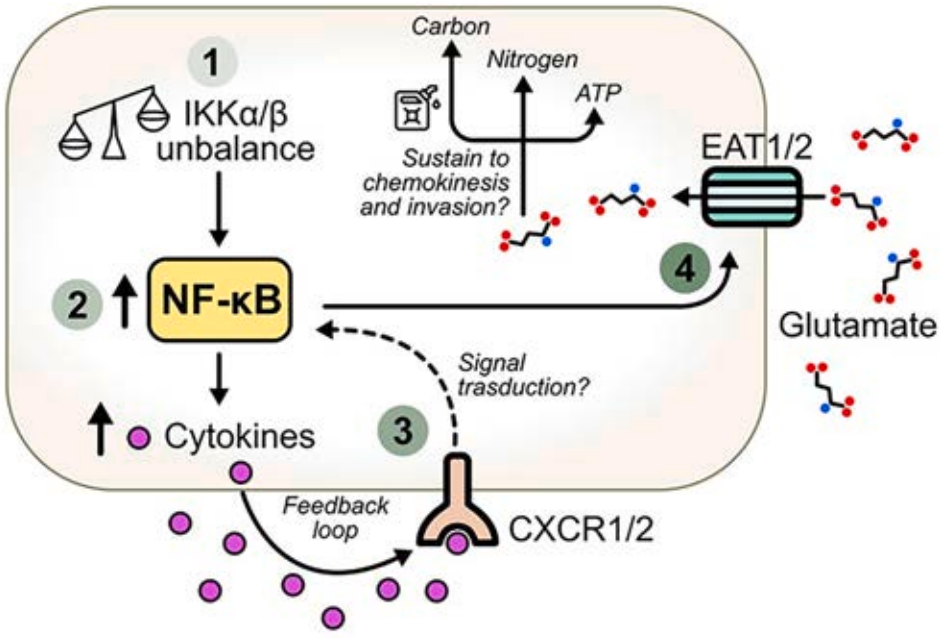

Fig. 7. NF-κB–mediated regulation of cytokine secretion and glutamate metabolism in brain-seeking breast cancer cells.
Brain-metastatic breast cancer cells acquire heightened NF-κB activity through the downregulation of IKKα and the upregulation of IKKβ (1), leading to its constitutive activation (2). This persistent NF-κB signaling drives the production of cytokines, which act through CXCR1/2 receptors (3), reinforcing a positive feedback loop that further sustains NF-κB activation. Additionally, constitutively active NF-κB induces the expression of glutamate transporters EAAT1/2, facilitating glutamate import into BrM cells, where it serves as a metabolic fuel that promotes tumor invasion and enhances chemokinesis (4).

regulatory influence via TAX1BP1. Intriguingly, the IKKβ homodimer may generate a unique signaling or transcriptional "signature" [29,48], leading to distinct cytokine production and potentially critical consequences for tumor progression. To explore this further, we experimentally modulated IKKα and IKKβ activity and monitored IL-8 expression over time. The resulting cytokine expression profiles were shaped not only by time, but also by the accumulation and biological impact of the overexpressed IKK variants. In our cellular model, which endogenously expresses low levels of IKKα and high levels of IKKβ, the introduction of IKKα-WT likely shifts the intracellular IKK composition, allowing for the formation of more IKKα/IKKβ heterodimers. These heterodimers are known to be more effective than IKKβ homodimers in promoting NF-κB-mediated transcription of pro-inflammatory genes [47], explaining the rapid early induction of IL-8 observed at 24 h. However, as IKKα accumulates over time, it also induces TAX1BP1, a negative regulator of NF-κB, which may account for the plateau observed at later time points. This biphasic effect, initial activation followed by feedback inhibition, is consistent with known properties of IKKα in immune signaling [49]. In contrast, IKKβ-DN inhibits both early and late NF-κB signaling events by stabilizing IκBα and promoting TAX1BP1 accumulation. This dual repression likely underlies the modest and flat IL-8 expression profile observed in this condition. Interestingly, the control cells, which lack exogenous modulation, show a more gradual yet sustained IL-8 induction. This trend likely reflects the natural progression of NF-κB signaling in a context where IKKβ activity predominates and no additional inhibitors are introduced. Overall, these findings highlight how modulating the balance and timing of IKKα and IKKβ activity, and their cumulative effects over time, critically shapes the amplitude and duration of the IL-8 response. We also analyzed the pattern of constitutively produced inflammatory cytokines in BrM cells compared to their parental counterparts. Human cells mainly produce IL-8 (absent in murine cells) and GRO-α, GRO-β, and GRO-γ, while murine BrM lines generate the homologs of GRO-α, GRO-β, and GRO-γ (Cxcl1, Cxcl2 and Cxcl3). These molecules appear to be involved in the metastatic process [50]. Notably, IL-8 was the most upregulated factor in a circulating tumor cell (CTC) database from patients with brain metastases (relative to those without metastases) [30]. Although IL-8 was previously linked indirectly to cerebral extravasation [51], the molecular details had remained unclear. Moreover IL-8 was also found to contribute to the formation of clusters between CTCs and neutrophils, which also play a role in metastasis [6]. Despite the limited patients sample in the reanalyzed database [30], inflammatory cytokines are clearly among the most overexpressed genes in CTCs from patients with brain metastases, validating our data on cell lines and supporting our overall premise. Two main extravasation mechanisms, paracellular and transcellular, have been identified for the blood-brain barrier (BBB) (see Ref. [52] for review). However, which route predominates during tumor cell passage across the BBB remains debated [53]. Many studies nonetheless indicate that paracellular invasion is directly involved, where endothelial junctions loosen and permit tumor cells to penetrate [54]. We have previously suggested that cancer cells might mimic immune-cell behavior. Immune cells normally infiltrate tissues during infections or other emergencies [6]. By hyperactivating inflammatory signaling (through IKKβ upregulation and IKKα downregulation), cancer cells can secrete large amounts of specific cytokines, emulating immune mechanisms yet using them to infiltrate tissues and establish metastases. The secreted cytokines [55], especially via CXCR1 and CXCR2 receptors on BBB endothelial cells [55], increase barrier permeability. Notably, iCXCR1/2, a single inhibitor, can block both CXCR1 and CXCR2 [56]. Conditioned media from the three BrM lines significantly increase dextran permeability, commonly used to assess BBB integrity with human brain endothelial cells (HCMEC/D3) [32], while iCXCR1/2 inhibits this effect, confirming that the identified cytokines primarily drive the permeabilization. Previous work has shown that cytokines secreted by immune cells can disrupt the BBB in instances of brain trauma, infection (for instance, viral or bacterial [57,58]) or systemic inflammation [59]. It is also well established that inflammatory cytokines significantly affect the metabolism of exposed cells. Immune cells, for example, adjust their metabolism upon activation, shifting metabolite usage according to nutrient availability [60]. In particular, NF-κB can be activated by different stimuli and contributes to metabolic regulation under pathological conditions. In pancreatic β cells, excess of glucose triggers increased intracellular Ca^{2+}, activating NF-κB and contributing to insulin secretion. Blocking NF-κB by overexpressing a non-degradable IκBα impairs glucose-stimulated insulin release [61]. Similarly, astrocytes modulate their metabolic processes in response to inflammatory factors like TNF and IL1-β, downregulating EAAT transporter transcription and activity for glutamate uptake [62]. This specific connection between inflammation and extracellular metabolites abundance in the brain underscores inflammation's broad impact on both cellular and tissue metabolism. Given the abundance of glutamate in the brain's extracellular environment and the relatively low amount of commonly used nutrients like glucose [35], it is logical to expect that metastatic cells will utilize the abundant metabolites during invasion [8]. Our data show that, in addition to cytokine production and BBB disruption, the altered NF-κB pathway drives metabolic adaptation in BrM cells. This pathway's over activation, both directly and via an autocrine mechanism involving CXCR1 and CXCR2 on BrM cells, upregulates glutamate transporters EAAT1 and EAAT2. The mechanism underlying this phenomenon could be simply explained by the presence of NF-κB regulatory binding sites in the promoters of both genes previously reported [63,64]. The inflammatory signals thus promote the use of glutamate by metastatic cells. Our metabolic data show that the upregulation of glutamate transporters leads to increased utilization of this metabolite by BrM cells compared to the parental cell line. Inhibition of glutamate uptake with iEAAT1/2 results in reduced respiration and, more significantly, a reduction in glycolysis. The effect on respiration could easily be explained by a decreased influx of glutamate into the Krebs cycle. The impact on glycolysis is less straightforward and could be attributed to the utilization of glutamate through the gluconeogenesis pathway, as observed in a comparable model where cells were directly injected into brain tissue [35]. The altered gluconeogenesis process appears essential for producing serine and pentose phosphates via specific metabolic pathways [35]. In our model, it can be hypothesized that excess gluconeogenesis is redirected to classical glycolysis when there is no further need for pentoses or serine [65]. Inhibition of glutamate uptake blocks this abnormal metabolic pathway, resulting in a marked reduction in glycolytic activity. Interestingly, the same type of analysis conducted using the IKKβ inhibitor shows, in specific conditions, even more dramatic results, suggesting the involvement of the inflammatory pathway not only in the metabolic mechanism related to glutamate but in a broader and more complex framework beyond the scope of this study. We have previously demonstrated the importance of extracellular amino acids in supporting chemokinesis and how lung cancer cells are extremely sensitive to even a minimal reduction in the uptake of amino acids like serine and glycine [9]. This sensitivity results in the complete cessation of migratory activity when the uptake of these specific amino acids is inhibited. Our migration and invasion experiments demonstrate that BrM cells increase their migratory capacity in the presence of higher levels of glutamate. The migratory process is inhibited when the glutamate import inhibitor is present, and the migration is even more dramatically blocked by the IKKβ inhibition. This suggests that after the BBB is made permeable by cytokines, the released glutamate is utilized by BrM cells to further enhance their migratory capacity. These cells exhibit exceptionally high levels of glutamate transporters, even exceeding those found in cells specialized for glutamate uptake, such as astrocytes, suggesting that they may act as effective competitors in glutamate uptake. The importance of glutamate in supporting breast cancer cell survival has been demonstrated previously, albeit through a completely different mechanism. Once cells have fully invaded the brain parenchyma, they develop a structure referred to as a "pseudosynapse," which utilizes extracellular

glutamate to activate the N-methyl-D-aspartate (NMDA) glutamate receptor. Although the details of this process remain unclear, this activation appears to support the survival of tumor cells within the brain parenchyma [66]. Our *in vivo* experiments further validate the critical role of glutamate uptake and utilization in driving tissue invasion. When mice inoculated via the carotid artery with 231BrM cells receive iEAAT1/2, they develop significantly fewer brain metastases compared to animals treated with PBS/DMSO alone.

These findings provide not only mechanistic insight but also potentially actionable therapeutic directions. For example, our demonstration that iEAAT1/2 treatment reduces brain metastasis burden highlights glutamate uptake as a promising pharmacological target. This opens the possibility of using glutamate transporter inhibitors such as DLTBOA in a perioperative context, specifically, in patients with a high risk of brain metastasis who are awaiting surgical removal of the primary tumor. Administering such inhibitors preoperatively could limit the metastatic potential of circulating tumor cells during this vulnerable window. Moreover, maintaining this treatment in the post-operative period might prevent residual circulating cells from seeding the brain, offering a novel prophylactic strategy for high-risk breast cancer patients. Future clinical studies could be designed to evaluate the feasibility, safety, and efficacy of such approaches.

5. Conclusions

Our findings reveal a novel inflammatory–metabolic axis in brain-seeking breast cancer cells, driven by constitutive NF-κB activation and enhanced glutamate metabolism. This axis promotes cytokine-mediated BBB disruption and supports tumor cell invasion and survival through increased glutamate uptake. Targeting key elements of this pathway, such as IKKβ, CXCR1/2 receptors, or glutamate transporters, effectively impairs metastatic progression and prevents brain colonization *in vivo*. These insights offer a broader understanding of the molecular strategies employed by metastatic cells to adapt to and thrive in the brain microenvironment. In particular, our work highlights how inflammatory signaling not only facilitates invasion but also reprograms cancer cell metabolism to exploit brain-specific resources. This dual role of NF-κB as both an inflammatory and metabolic driver positions it as a central node in metastasis biology. Furthermore, the identification of converging inflammatory and metabolic vulnerabilities paves the way for multi-target therapeutic approaches, potentially combining inhibitors of cytokine signaling with metabolic modulators to enhance treatment efficacy. As brain metastases remain a major clinical challenge with limited therapeutic options, our study contributes valuable preclinical evidence to support the development of preventive and adjunct therapies for high-risk breast cancer patients.

CRediT authorship contribution statement

Sara Di Russo: Investigation, Data curation. **Giulia Elizabeth Borsatti:** Investigation. **Amani Bouzidi:** Investigation. **Francesca Romana Liberati:** Investigation. **Agnese Riva:** Investigation. **Farida Tripodi:** Methodology, Investigation. **Lucrezia Romana Rolfi:** Methodology, Investigation, Funding acquisition. **Sharon Spizzichino:** Investigation. **Antonella Tramutola:** Methodology, Investigation. **Marzia Perluigi:** Supervision, Funding acquisition. **Daniela Trisciuoglio:** Methodology, Investigation, Funding acquisition, Formal analysis, Data curation. **Giorgio Giardina:** Visualization. **Alessandro Paiardini:** Software, Funding acquisition, Formal analysis, Data curation. **Paola Coccetti:** Supervision, Funding acquisition. **Serena Rinaldo:** Writing – review & editing, Funding acquisition. **Francesca Cutruzzolà:** Writing – review & editing, Supervision, Funding acquisition. **Alessio Paone:** Writing – review & editing, Writing – original draft, Supervision, Methodology, Funding acquisition, Conceptualization.

Ethics approval statement

All procedures involving animals were performed in strict accordance with protocols authorized by the Italian Ministry of Health. Detailed information, including the specific approval numbers, can be found in the Materials and Methods section.

Data availability statement

The data that support the findings of this study are available from the corresponding author upon reasonable request.

Author statement on the use of AI tools

Artificial intelligence (Scholar GPT) was used exclusively to refine language clarity. All scientific content, data interpretation, and conclusions were generated by the authors. Every detail of the manuscript has been thoroughly reviewed and validated by the corresponding author prior to submission.

Funding

This work was supported by grants from Sapienza University research grants: RP1221816B26A29B, RP12117A675EDA46, RP120172B85FA568 (to A.P.), RM1221815D52AB32 (to A. Paia.), RM12117A5BDD4AEC (to G.G.), RD12318AA8EEA45D (to the department of Biochemical Sciences A, Rossi Fanelli), RG123188B0602C40 and RM11916B46D48441 (to F.C.), Grandi Attrezzature Scientifiche 2021 n. GA116154C8A94E3D (to F.C.). Associazione Italiana Ricerca sul Cancro (AIRC) IG2019 n. 23,125 (to F.C.) and IG 2020 n.24,942 to (D. T.). Ministry of Health, grant RF-2019-12368888 (to F.C.), European Union – NextGenerationEU": DD. 3175/2021 E DD. 3138/2021 CN_3: National 478 Center for Gene Therapy and Drugs based on RNA Technology- Project CN 00000041 (to F.C.Supporting S. DR). MIUR PRIN 2022 grant number 20228395 KW (to F.C.), Italian Ministry of University and research 2024-ATE-031 (to P.C.), Italy Ministry of University and Research PRIN [CUP: 2022N3JXLA] (to A. Paia.). Fondazione Neuroblastoma 2024 - [Cod. Project: VAMOLAA] (to A. Paia.). Istituto Pasteur Fondazione Cenci Bolognetti, Anna Tramontano research project 2022 (to M.P.). EuropeanUnion – NextGenerationEU (Project ECS 0000024Rome Technopole, – CUP B83C22002820006, NRP Mission 4 Component 2 Investment 1.5 to LRR) National Recovery and Resilience Plan (NRRP), Mission 4, Component 2, Investment 1.1, Call No. 104 (February 2, 2022) by the Italian Ministry of University and Research (MUR), funded by the European Union – NextGenerationEU Project N. CUP N. B53D23016330006 (to S.R.). The authors gratefully acknowledge all the funding sources reported for their valuable support.

Declaration of competing interest

The authors declare that they have no competing interests.

Acknowledgements

We sincerely thank Prof. Joan Massagué for kindly providing the 231BrM cells and their counterpart, Prof. Manuel Valiente for generously providing the E0771BrM cells and their counterpart, and Prof. Mihaela Lorger for kindly supplying the 4T1 cells and their counterpart. We gratefully acknowledge Prof. Loretta Tuosto for generously providing the IKKα and IKKβ-DN plasmids and Dr. Giovanna Boumis for her constant and invaluable support.

Appendix A. Supplementary data

Supplementary data to this article can be found online at https://doi.org/10.1016/j.canlet.2025.217907.

References

[1] R.L. Siegel, A.N. Giaquinto, A. Jemal, Cancer statistics, CA Cancer J. Clin. 74 (2024), https://doi.org/10.3322/caac.21820, 2024.

[2] M. Kuksis, Y. Gao, W. Tran, C. Hoey, A. Kiss, A.S. Komorowski, A.J. Dhaliwal, A. Sahgal, S. Das, K.K. Chan, K.J. Jerzak, The incidence of brain metastases among patients with metastatic breast cancer: a systematic review and meta-analysis, Neuro Oncol. 23 (2021), https://doi.org/10.1093/neuonc/noaa285.

[3] M. Masmudi-Martín, L. Zhu, M. Sanchez-Navarro, N. Priego, M. Casanova-Acebes, V. Ruiz-Rodado, E. Giralt, M. Valiente, Brain metastasis models: what should we aim to achieve better treatments? Adv. Drug Deliv. Rev. 169 (2021) https://doi.org/10.1016/j.addr.2020.12.002.

[4] J. Fares, A. Cordero, D. Kanojia, M.S. Lesniak, The network of cytokines in brain metastases, Cancers (Basel) 13 (2021), https://doi.org/10.3390/cancers13010142.

[5] C. Agnoletto, F. Corrà, L. Minotti, F. Baldassari, F. Crudele, W.J.J. Cook, G. Di Leva, A.P. D'Adamo, P. Gasparini, S. Volinia, Heterogeneity in circulating tumor cells: the relevance of the stem-cell subset, Cancers (Basel) 11 (2019), https://doi.org/10.3390/cancers11040483.

[6] S. Di Russo, F.R. Liberati, A. Riva, F. Di Fonzo, A. Macone, G. Giardina, M. Arese, S. Rinaldo, F. Cutruzzolà, A. Paone, Beyond the barrier: the immune-inspired pathways of tumor extravasation, Cell Commun. Signal. 22 (2024), https://doi.org/10.1186/s12964-023-01429-1.

[7] M. Martinez, A. Frank, E. Diez-Tejedor, A. Hernanz, Amino acid concentrations in cerebrospinal fluid and serum in Alzheimer's disease and vascular dementia, J. Neural Transm. Park. Dis. Dement. Sect. 6 (1993), https://doi.org/10.1007/BF02252617.

[8] F. Cutruzzolà, A. Bouzidi, F.R. Liberati, S. Spizzichino, G. Boumis, A. Macone, S. Rinaldo, G. Giardina, A. Paone, The emerging role of amino acids of the brain microenvironment in the process of metastasis formation, Cancers (Basel) (2021), https://doi.org/10.3390/cancers13122891.

[9] A. Bouzidi, M.C. Magnifico, A. Paiardini, A. Macone, G. Boumis, G. Giardina, S. Rinaldo, F.R. Liberati, C. Lauro, C. Limatola, C. Lanzillotta, A. Tramutola, M. Perluigi, G. Sgarbi, G. Solaini, A. Baracca, A. Paone, F. Cutruzzolà, Cytosolic serine hydroxymethyltransferase controls lung adenocarcinoma cells migratory ability by modulating AMP kinase activity, Cell Death Dis. (2020), https://doi.org/10.1038/s41419-020-03215-0.

[10] P.D. Bos, X.H.F. Zhang, C. Nadal, W. Shu, R.R. Gomis, D.X. Nguyen, A.J. Minn, M. J. Van De Vijver, W.L. Gerald, J.A. Foekens, J. Massagué, Genes that mediate breast cancer metastasis to the brain, Nature 459 (2009), https://doi.org/10.1038/nature08021.

[11] M. Lorger, B. Felding-Habermann, Capturing changes in the brain microenvironment during initial steps of breast cancer brain metastasis, Am. J. Pathol. 176 (2010), https://doi.org/10.2353/ajpath.2010.090838.

[12] C. Monteiro, L. Miarka, M. Perea-García, N. Priego, P. García-Gómez, L. Álvaro-Espinosa, A. de Pablos-Aragoneses, N. Yebra, D. Retana, P. Baena, C. Fustero-Torre, O. Graña-Castro, K. Troulé, E. Caleiras, P. Tezanos, P. Muela, E. Cintado, J.L. Trejo, J.M. Sepúlveda, P. González-León, L. Jiménez-Roldán, L.M. Moreno, O. Esteban, Á. Pérez-Núñez, A. Hernández-Lain, J. Mazarico Gallego, I. Ferrer, R. Suárez, E. M. Garrido-Martín, L. Paz-Ares, C. Dalmasso, E. Cohen-Jonathan Moyal, A. Siegfried, A. Hegarty, S. Keelan, D. Vareslija, L.S. Young, M. Mohme, Y. Goy, H. Wikman, J. Fernández-Alén, G. Blasco, L. Alcázar, C. Cabañuz, S.I. Grivennikov, A. Ianus, N. Shemesh, C.C. Faria, R. Lee, P. Lorigan, E. Le Rhun, M. Weller, R. Soffietti, L. Bertero, U. Ricardi, J. Bosch-Barrera, E. Sais, E. Teixidor, A. Hernández-Martínez, A. Calvo, J. Aristu, S.M. Martin, A. Gonzalez, O. Adler, N. Erez, C. Sobrino, N. Ajenjo, M.J. Artiga, E. Ortega-Paino, M. Valiente, Stratification of radiosensitive brain metastases based on an actionable S100A9/RAGE resistance mechanism, Nat. Med. 28 (2022), https://doi.org/10.1038/s41591-022-01749-8.

[13] F. Tripodi, Z. Motta, G. Murtas, V. Rabattoni, S. Nonnis, F. Grassi Scalvini, A. M. Rinaldi, R. Rizzi, C. Bearzi, B. Badone, S. Sacchi, G. Tedeschi, E. Maffioli, P. Coccetti, L. Pollegioni, Serine metabolism during differentiation of human iPSC-derived astrocytes, FEBS J. 290 (2023), https://doi.org/10.1111/febs.16816.

[14] A. De Corato, L. Lisi, A. Capuano, G. Tringali, A. Tramutola, P. Navarra, C. Dello Russo, Trigeminal satellite cells express functional calcitonin gene-related peptide receptors, whose activation enhances interleukin-1β pro-inflammatory effects, J. Neuroimmunol. 237 (2011), https://doi.org/10.1016/j.jneuroim.2011.05.013.

[15] D. Starace, R. Galli, A. Paone, P. De Cesaris, A. Filippini, E. Ziparo, A. Riccioli, Toll-like receptor 3 activation induces antiviral immune responses in mouse sertoli cells, Biol. Reprod. 79 (2008), https://doi.org/10.1095/biolreprod.108.068619.

[16] G. Guiducci, A. Paone, A. Tramonti, G. Giardina, S. Rinaldo, A. Bouzidi, M. C. Magnifico, M. Marani, J.A. Menendez, A. Fatica, A. MacOne, A. Armaos, G. G. Tartaglia, R. Contestabile, A. Paiardini, F. Cutruzzol, The moonlighting RNA-Binding activity of cytosolic serine hydroxymethyltransferase contributes to control compartmentalization of serine metabolism, Nucleic Acids Res. 47 (2019) 4240, https://doi.org/10.1093/NAR/GKZ129.

[17] C. Zhang, F.J. Lowery, D. Yu, Intracarotid cancer cell injection to produce mouse models of brain metastasis, J. Vis. Exp. (2017), https://doi.org/10.3791/55085.

[18] A. Al Shoyaib, S.R. Archie, V.T. Karamyan, Intraperitoneal route of drug administration: should it be used in experimental animal studies? Pharm. Res. (2020) https://doi.org/10.1007/s11095-019-2745-x.

[19] E. Piccolella, F. Spadaro, C. Ramoni, B. Marinari, A. Costanzo, M. Levrero, L. Thomson, R.T. Abraham, L. Tuosto, Vav-1 and the IKKα subunit of IκB kinase functionally associate to induce NF-κB activation in response to CD28 engagement, J. Immunol. 170 (2003), https://doi.org/10.4049/jimmunol.170.6.2895.

[20] R.M. Burnett, K.E. Craven, P. Krishnamurthy, C.P. Goswami, S. Badve, P. Crooks, W.P. Mathews, P. Bhat-Nakshatri, H. Nakshatri, Organ-specific adaptive signaling pathway activation in metastatic breast cancer cells, Oncotarget 6 (2015), https://doi.org/10.18632/oncotarget.3707.

[21] L.A. Solt, M.J. May, The IκB kinase complex: master regulator of NF-κB signaling, Immunol. Res. 42 (2008), https://doi.org/10.1007/s12026-008-8025-1.

[22] J.A. Prescott, J.P. Mitchell, S.J. Cook, Inhibitory feedback control of NF-?B signalling in health and disease, Biochem. J. 478 (2021), https://doi.org/10.1042/BCJ20210139.

[23] N.G. Anthony, J. Baiget, G. Berretta, M. Boyd, D. Breen, J. Edwards, C. Gamble, A. I. Gray, A.L. Harvey, S. Hatziieremia, K.H. Ho, J.K. Huggan, S. Lang, S. Llona-Minguez, J.L. Luo, K. McIntosh, A. Paul, R.J. Plevin, M.N. Robertson, R. Scott, C. J. Suckling, O.B. Sutcliffe, L.C. Young, S.P. Mackay, Inhibitory kappa B kinase α (IKKα) inhibitors that recapitulate their selectivity in cells against isoform-related biomarkers, J. Med. Chem. 60 (2017), https://doi.org/10.1021/acs.jmedchem.7b00484.

[24] X. Wang, S.R. Naidu, F. Sverdrup, E.J. Androphy, Tax1BP1 interacts with papillomavirus E2 and regulates E2-Dependent transcription and stability, J. Virol. 83 (2009), https://doi.org/10.1128/jvi.01791-08.

[25] D.S. Petkova, P. Verlhac, A. Rozières, J. Baguet, M. Claviere, C. Kretz-Remy, R. Mahieux, C. Viret, M. Faure, Distinct contributions of autophagy receptors in measles virus replication, Viruses 9 (2017), https://doi.org/10.3390/v9050123.

[26] Y.B. Choi, J. Zhang, M.T. Vo, J. White, C. He, E.W. Harhaj, Phosphorylation of the selective autophagy receptor TAX1BP1 by canonical and noncanonical IκB kinases promotes its lysosomal localization and clearance of MAVS aggregates, bioRxiv (2021).

[27] N. Shembade, R. Pujari, N.S. Harhaj, D.W. Abbott, E.W. Harhaj, The kinase IKKα inhibits activation of the transcription factor NF-κB by phosphorylating the regulatory molecule TAX1BP1, Nat. Immunol. 12 (2011), https://doi.org/10.1038/ni.2066.

[28] A. Page, M. Navarro, M. Garín, P. Pérez, M.L. Casanova, R. Moreno, J.L. Jorcano, J. L. Cascallana, A. Bravo, A. Ramírez, IKKB leads to an inflammatory skin disease resembling interface dermatitis, J. Invest. Dermatol. 130 (2010), https://doi.org/10.1038/jid.2010.28.

[29] F. Mercurio, B.W. Murray, A. Shevchenko, B.L. Bennett, D.B. Young, J.W. Li, G. Pascual, A. Motiwala, H. Zhu, M. Mann, A.M. Manning, IκB kinase (IKK)-associated protein 1, a common component of the heterogeneous IKK complex, Mol. Cell Biol. 19 (1999), https://doi.org/10.1128/mcb.19.2.1526.

[30] D. Boral, M. Vishnoi, H.N. Liu, W. Yin, M.L. Sprouse, A. Scamardo, D.S. Hong, T. Z. Tan, J.P. Thiery, J.C. Chang, D. Marchetti, Molecular characterization of breast cancer CTCs associated with brain metastasis, Nat. Commun. 8 (2017), https://doi.org/10.1038/s41467-017-00196-1.

[31] B. Weksler, I.A. Romero, P.O. Couraud, The hCMEC/D3 cell line as a model of the human blood brain barrier, Fluids Barriers CNS (2013), https://doi.org/10.1186/2045-8118-10-16.

[32] C. Förster, M. Burek, I.A. Romero, B. Weksler, P.O. Couraud, D. Drenckhahn, Differential effects of hydrocortisone and TNFα on tight junction proteins in an in vitro model of the human blood-brain barrier, J. Physiol. 586 (2008), https://doi.org/10.1113/jphysiol.2007.146852.

[33] S. Sitaru, A. Budke, R. Bertini, M. Sperandio, Therapeutic inhibition of CXCR1/2: where do we stand? Intern. Emerg. Med. 18 (2023) https://doi.org/10.1007/s11739-023-03309-5.

[34] C. Sticozzi, G. Belmonte, M. Frosini, F. Pessina, Nitric oxide/cyclic GMP-dependent calcium signalling mediates IL-6- and TNF-α-Induced expression of glial fibrillary acid protein, J. Mol. Neurosci. 71 (2021), https://doi.org/10.1007/s12031-020-01708-3.

[35] J. Chen, H.J. Lee, X. Wu, L. Huo, S.J. Kim, L. Xu, Y. Wang, J. He, L.R. Bollu, G. Gao, F. Su, J. Briggs, X. Liu, T. Melman, J.M. Asara, I.J. Fidler, L.C. Cantley, J. W. Locasale, Z. Weihua, Gain of glucose-independent growth upon metastasis of breast cancer cells to the brain, Cancer Res. (2015), https://doi.org/10.1158/0008-5472.CAN-14-2268.

[36] H. Basun, L.G. Forssell, O. Almkvist, R.F. Cowburn, R. Eklöf, B. Winblad, L. Wetterberg, Amino acid concentrations in cerebrospinal fluid and plasma in Alzheimer's disease and healthy control subjects, J. Neural Transm. Park. Dis. Dement. Sect. (1990), https://doi.org/10.1007/BF02252924.

[37] S. Mahmoud, M. Gharagozloo, C. Simard, D. Gris, Astrocytes maintain glutamate homeostasis in the cns by controlling the balance between glutamate uptake and release, Cells 8 (2019), https://doi.org/10.3390/cells8020184.

[38] S. Grivennikov, M. Karin, Autocrine IL-6 signaling: a key event in tumorigenesis? Cancer Cell 13 (2008) https://doi.org/10.1016/j.ccr.2007.12.020.

[39] W. Fu, Y. Zhang, J. Zhang, W.F. Chen, Cloning and characterization of mouse homolog of the CXC chemokine receptor CXCR1, Cytokine 31 (2005), https://doi.org/10.1016/j.cyto.2005.02.005.

[40] S. Uttam, C. Wong, T.J. Price, A. Khoutorsky, eIF4E-Dependent translational control: a central mechanism for regulation of pain plasticity, Front. Genet. 9 (2018), https://doi.org/10.3389/fgene.2018.00470.

[41] K. Shimamoto, R. Sakai, K. Takaoka, N. Yumoto, T. Nakajima, S.G. Amara, Y. Shigeri, Characterization of novel L-threo-β-Benzyloxyaspartate derivatives, potent blockers of the glutamate transporters, Mol. Pharmacol. (2004), https://doi.org/10.1124/mol.65.4.1008.

[42] D. Capece, D. Verzella, I. Flati, P. Arboretto, J. Cornice, G. Franzoso, NF-κB: blending metabolism, immunity, and inflammation, Trends Immunol. 43 (2022), https://doi.org/10.1016/j.it.2022.07.004.

[43] A.J. Minn, G.P. Gupta, P.M. Siegel, P.D. Bos, W. Shu, D.D. Giri, A. Viale, A. B. Olshen, W.L. Gerald, J. Massagué, Genes that mediate breast cancer metastasis to lung, Nature (2005), https://doi.org/10.1038/nature03799.

[44] M. Żebrowska-Nawrocka, D. Szmajda-Krygier, A. Krygier, A. Jeleń, E. Balcerczak, Bioinformatic analysis of IKK complex genes expression in selected gastrointestinal cancers, Int. J. Mol. Sci. 25 (2024) 9868, https://doi.org/10.3390/ijms25189868.
[45] N. Shembade, N.S. Harhaj, D.J. Liebl, E.W. Harhaj, Essential role for TAX1BP1 in the termination of TNF-α-, IL-1- and LPS-mediated NF-κB and JNK signaling, EMBO J. 26 (2007), https://doi.org/10.1038/sj.emboj.7601823.
[46] M. Adli, E. Merkhofer, P. Cogswell, A.S. Baldwin, IKKα and IKKβ each function to regulate NF-κB activation in the TNF-induced/canonical pathway, PLoS One 5 (2010), https://doi.org/10.1371/journal.pone.0009428.
[47] J.A. Prescott, K. Balmanno, J.P. Mitchell, H. Okkenhaug, S.J. Cook, IKKα plays a major role in canonical NF-κB signalling in colorectal cells, Biochem. J. 479 (2022), https://doi.org/10.1042/BCJ20210783.
[48] S. Polley, D. Bin Huang, A.V. Hauenstein, A.J. Fusco, X. Zhong, D. Vu, B. Schröfelbauer, Y. Kim, A. Hoffmann, I.M. Verma, G. Ghosh, T. Huxford, A structural basis for IκB kinase 2 activation via oligomerization-dependent trans auto-phosphorylation, PLoS Biol. 11 (2013), https://doi.org/10.1371/journal.pbio.1001581.
[49] B. Chatterjee, P. Roy, U.A. Sarkar, M. Zhao, Y. Ratra, A. Singh, M. Chawla, S. De, J. Gomes, R. Sen, S. Basak, Immune differentiation regulator p100 tunes NF-κB responses to TNF, Front. Immunol. 10 (2019), https://doi.org/10.3389/fimmu.2019.00997.
[50] V. Hannelien, G. Karel, V.D. Jo, S. Sofie, The role of CXC chemokines in the transition of chronic inflammation to esophageal and gastric cancer, Biochim. Biophys. Acta Rev. Canc 1825 (2012), https://doi.org/10.1016/j.bbcan.2011.10.008.
[51] O. Benchama, S. Tyukhtenko, M.S. Malamas, M.K. Williams, A. Makriyannis, H. K. Avraham, Inhibition of triple negative breast cancer-associated inflammation, tumor growth and brain colonization by targeting monoacylglycerol lipase, Sci. Rep. 12 (2022), https://doi.org/10.1038/s41598-022-09358-8.
[52] B. McDonald, K. Barth, M.H.H. Schmidt, The origin of brain malignancies at the blood–brain barrier, Cell. Mol. Life Sci. 80 (2023), https://doi.org/10.1007/s00018-023-04934-1.
[53] C.D. Arvanitis, G.B. Ferraro, R.K. Jain, The blood–brain barrier and blood–tumour barrier in brain tumours and metastases, Nat. Rev. Cancer (2020), https://doi.org/10.1038/s41568-019-0205-x.
[54] J.J. Connell, G. Chatain, B. Cornelissen, K.A. Vallis, A. Hamilton, L. Seymour, D. C. Anthony, N.R. Sibson, Selective permeabilization of the blood-brain barrier at sites of metastasis, J. Natl. Cancer Inst. 105 (2013), https://doi.org/10.1093/jnci/djt276.
[55] I.U. Schraufstatter, J. Chung, M. Burger, IL-8 activates endothelial cell CXCR1 and CXCR2 through rho and rac signaling pathways, Am. J. Physiol. Lung Cell. Mol. Physiol. 280 (2001), https://doi.org/10.1152/ajplung.2001.280.6.l1094.
[56] K. Boon, N. Vanalken, M. Szpakowska, A. Chevigné, D. Schols, T. Van Loy, Systematic assessment of chemokine ligand bias at the human chemokine receptor CXCR2 indicates G protein bias over β-arrestin recruitment and receptor internalization, Cell Commun. Signal. 22 (2024), https://doi.org/10.1186/s12964-023-01460-2.
[57] J.M.M. Al-Obaidi, A. Bahadoran, S.M. Wang, R. Manikam, C.S. Raju, S.D. Sekaran, Disruption of the blood brain barrier is vital property of neurotropic viral infection of the central nervous system, Acta Virol. 62 (2018), https://doi.org/10.4149/av_2018_102.
[58] T. Barichello, J.S. Pereira, G.D. Savi, J.S. Generoso, A.L. Cipriano, C. Silvestre, F. Petronilho, F. Dal-Pizzol, M.C. Vilela, A.L. Teixeira, A kinetic study of the cytokine/chemokines levels and disruption of blood-brain barrier in infant rats after pneumococcal meningitis, J. Neuroimmunol. 233 (2011), https://doi.org/10.1016/j.jneuroim.2010.10.035.
[59] A. Varatharaj, I. Galea, The blood-brain barrier in systemic inflammation, Brain Behav. Immun. 60 (2017), https://doi.org/10.1016/j.bbi.2016.03.010.
[60] L. Sun, X. Yang, Z. Yuan, H. Wang, Metabolic reprogramming in immune response and tissue inflammation, Arterioscler. Thromb. Vasc. Biol. 40 (2020), https://doi.org/10.1161/ATVBAHA.120.314037.
[61] M. Kracht, U. Müller-Ladner, M.L. Schmitz, Mutual regulation of metabolic processes and proinflammatory NF-κB signaling, J. Allergy Clin. Immunol. 146 (2020), https://doi.org/10.1016/j.jaci.2020.07.027.
[62] J. Liang, H. Takeuchi, Y. Doi, J. Kawanokuchi, Y. Sonobe, S. Jin, I. Yawata, H. Li, S. Yasuoka, T. Mizuno, A. Suzumura, Excitatory amino acid transporter expression by astrocytes is neuroprotective against microglial excitotoxicity, Brain Res. 1210 (2008), https://doi.org/10.1016/j.brainres.2008.03.012.
[63] Z. zhong Su, M. Leszczyniecka, D. chul Kang, D. Sarkar, W. Chao, D.J. Volsky, P. B. Fisher, Insights into glutamate transport regulation in human astrocytes: cloning of the promoter for excitatory amino acid transporter 2 (EAAT2), Proc. Natl. Acad. Sci. USA. 100 (2003), https://doi.org/10.1073/pnas.0136555100.
[64] S.Y. Kim, S.Y. Choi, W. Chao, D.J. Volsky, Transcriptional regulation of human excitatory amino acid transporter 1 (EAAT1): cloning of the EAAT1 promoter and characterization of its basal and inducible activity in human astrocytes, J. Neurochem. 87 (2003), https://doi.org/10.1046/j.1471-4159.2003.02128.x.
[65] B. Chaneton, P. Hillmann, L. Zheng, A.C.L. Martin, O.D.K. Maddocks, A. Chokkathukalam, J.E. Coyle, A. Jankevics, F.P. Holding, K.H. Vousden, C. Frezza, M. O'Reilly, E. Gottlieb, Serine is a natural ligand and allosteric activator of pyruvate kinase M2, Nature 491 (2012), https://doi.org/10.1038/nature11540.
[66] Q. Zeng, I.P. Michael, P. Zhang, S. Saghafinia, G. Knott, W. Jiao, B.D. McCabe, J. A. Galván, H.P.C. Robinson, I. Zlobec, G. Ciriello, D. Hanahan, Synaptic proximity enables NMDAR signalling to promote brain metastasis, Nature (2019), https://doi.org/10.1038/s41586-019-1576-6.

Glossary

BBB –: Blood-Brain Barrier
BrM –: Brain Metastatic
MBC –: Metastatic Breast Cancer
CTC –: Circulating Tumor Cell
NF-κB –: Nuclear Factor kappa-light-chain-enhancer of activated B cells
IκBα –: Inhibitor of NF-κB alpha
TAX1BP1 –: Tax1 Binding Protein 1
CXCR1/2 –: C-X-C Motif Chemokine Receptor 1/2
EAAT1/2 –: Excitatory Amino Acid Transporter 1/2
IL-8 –: Interleukin 8
GRO –: Growth-Regulated Oncogene
OCR –: Oxygen Consumption Rate
ECAR –: Extracellular Acidification Rate
ELISA –: Enzyme-Linked Immunosorbent Assay
RNAi –: RNA interference
iIKKβ –: IKKβ Inhibitor
iEAAT1/2 –: EAAT1/2 Inhibitor
iCXCR1/2 –: CXCR1/2 Inhibitor
GFAP –: Glial Fibrillary Acidic Protein
BEF –: Brain Extracellular Fluid
IVIS –: In Vivo Imaging System